

Requested minor revisions to gmd-2019-196

Dear Lauren Gregoire,

We are very pleased about your decision about the manuscript.

We also thank you for the new comments you addressed. Please see our reply.

L228: Clarify the procedure for boundary conditions applied when running NEMO ocean only model. This paragraph is currently too vague and it's difficult to make sense of it. Clarify what the flux are, what the restoring term is and what the constant coefficient controls. If there is a paper you can cite that would be great, otherwise please include an equation.

Indeed, that the flux and restoring term comes from Barnier et al., 1995, we inserted the reference in the new version of the manuscript (L226 and L715).

L306: "The global simulation, after SST bias correction, ranged with the observation, compared to IPSLCM5A (Figure 2)." "ranged with the observation" is not clear. Do you mean "has the same range of variability as e.g. the 2m temperature over the Mediterranean region from ERA20C" ?

We apologize that there was a misunderstanding in our results description. Actually, the line you mentioned only describes the global average of 2m temperature and it is not related to the Mediterranean. We suspect that the word "range" was inappropriately used. We made the necessary changes in the new manuscript. By the way, we also make a slight change for the regional aspect over the Mediterranean:

L302

Previous sentence: "The global simulation, after SST bias correction, ranged with the observation, compared to IPSLCM5A (Figure 2)"

New sentence: "The global simulation (continued red curve in Fig. 2), after SST bias correction, is very close to the observation (continued black curve), with a tremendous improvement compared to IPSLCM5A (green curve in Figure 2)." The regional model reproduces the warming trend and aspects of the interannual variability close to observations, **but with a mean cold shift of about -0.6°C.**

L219 "A first dataset of climatological river discharges is proposed by default to cover the entire Mediterranean draining basin with represents 33 river mouths." What do you mean by "is proposed" to whom, for what? How is it used? Please clarify the text.

We apologize again for the confusion. Actually, that dataset of rivers freshwater discharges was constructed by the initial NEMOMED model developers, and was proposed to us (authors of the manuscript) to be used if we don't include the rivers interactively. We changed this paragraph into past tense ("is" to "was", L216), which can help to remove the confusion. "A dataset of climatological river discharges was proposed by default within the NEMOMED8 platform to cover the entire Mediterranean draining basin with 33 river mouths."

"[Reviewer comment]"

P7 lines 211-213: how realistic is the assumption that water from the Black Sea is fresh? And does the Q+P-E budget over the Black Sea derive from the AGCM or ARCM?

[Reply]

It is a commonly-used treatment when the Mediterranean model doesn't include the Black Sea. The fresh water assumption is entirely justified although the actual water flow from the Black Sea can be salty, since what we evaluated in terms of E, P and Runoff is indeed the fresh water budget. What is important in the model is not the water mass itself, but the salt content. We made some revisions in the new manuscript for this regard."

I can't see how and where you have addressed this point. Please clarify with citation of the text.

For this purpose, we update the text at l221 "The Black Sea fresh water assumption comes from NEMOMED modeling community that consider it as a yearly source of freshwater" and l450 "For this part, the water budget over the Black Sea is calculated from the ARCM output"

"[Reviewer comment]

P14 lines 362-364: Figures 2 and 4 show that your simulation results in significantly lower temperatures than observed, yet here you say they are consistent?

[Reply]

Yes, there are cold biases. We changed the corresponding text in the revised manuscript "The atmospheric simulation is acceptable compared with observations for the air temperature at 2m at both global and regional scales "(l405)."

I am not satisfied with how you have addressed this point. Changing the word "consistent" with "acceptable" just makes a wrong statement into something vague and subjective. Please quantify and describe the cold bias and discuss the implications here.

Indeed, we made the following correction l417: "Validation of our platform was based on the historical period from 1970 to 1999. after bias correction of global SST, the 2-m surface air temperature in the HIST global simulation is comparable to the observational counterpart. However, the simulated surface air temperature within the regional model is colder (as shown in Figure 2), which implies SST cold biases for the Mediterranean Sea"

"[Reviewer comment]

P22, lines 522-525: what do you mean by the reference for correction is the preindustrial state? How is river runoff corrected based on pre-industrial climate?

[Reply]

We choose to "correct" the Mediterranean river runoff during the Early Holocene based on the precipitation difference (EHOL – PICTRL) coming from both the ARCM and AGCM and apply it to the PICTRL river runoff (which was prescribed). The procedure of river runoff is detailed in the supplementary material (**Text S2: Bias correction**)"

This point hasn't been addressed adequately, please correct the text when you make reference to the "correction" to clarify that you apply a bias correct as described in Text S2.

If we understand well, we just need to clarify the response in the manuscript l593. « The procedure of river runoff is detailed in the supplementary material (Text S2: Bias correction) »

Editorial corrections (suggested changes in bold):

Thanks, we took all of these suggestions into account.

~~L153: “This architecture is based on a method **that provides** as much **compatibility** as possible amongst the models used and high **consistency** with data.”~~

~~L224L “river mouths **that** cover the ...”~~

~~L330 “ both the precipitation and evaporation over the Mediterranean Sea in HIST **are** very close to the observations”~~ Quantify how close.

L331 “but both the precipitation and evaporation over the Mediterranean Sea in HIST are very close to the observations, **with 10 mm.yr⁻¹ of oceanic precipitation difference between HIST and the mean observation value (by taking the upper and the lower value), and 18 mm.yr⁻¹ for the oceanic evaporation.**”

~~L331 “**The** two other simulations **included in Table 1**, PICTRL and EHOL, are those designed to investigate the Early Holocene climate **(see Section 4).**”~~

~~L407: “The ZOF in HIST depicted in Figure 6)”~~

Figure 6: replace row numbers with figure labels (a-h)

~~L425 It is not correct to say “ranges with the observation”. Do you mean “has the same range of variability as the observations”~~

Please see the new version of the main manuscript, the supplement remains unchanged.

Regards

Tristan Vadsaria on Behalf of all co-authors

Added reference L715:

Barnier, B., Siefridt, L. and Marchesio, P.: Thermal forcing for a global ocean circulation model using a three-year climatology of ECMWF analyses, J. Mar. Syst., 6(4), 363–380, doi:10.1016/0924-7963(94)00034-9, 1995.

Development of a sequential tool, LMDZ-NEMO-med-V1, to conduct global to regional past climate simulation for the Mediterranean basin: An Early Holocene case study

Tristan Vadsaria^{1,3}, Laurent Li², Gilles Ramstein¹ and Jean-Claude Dutay¹

¹Laboratoire des Sciences du Climat et de l'Environnement, CEA-CNRS- Université Paris Saclay, Gif-sur-Yvette, 91191, France

²Laboratoire de Météorologie Dynamique, CNRS-ENS-Ecole Polytechnique- Sorbonne Université, Paris, 75005, France

³Atmosphere and Ocean Research Institute, University of Tokyo, Kashiwanoha, Chiba, Japan

Correspondence to: Tristan Vadsaria (tristan.vadsaria@lscce.ipsl.fr)

Abstract

Recently, major progress has been made in the simulation of the ocean dynamics of the Mediterranean using atmospheric and oceanic models with high spatial resolution. High resolution is essential to accurately capture the synoptic variability required to initiate intermediate and deep-water formation, the engine of the MTC (Mediterranean Thermohaline Circulation). In paleoclimate studies, one major problem with the simulation of regional climate changes is that boundary conditions are not available from observations or data reconstruction to drive high-resolution regional models. One consistent way to advance paleoclimate modelling is to use a comprehensive global to regional approach. However, this approach needs long-term integration to reach equilibrium (hundreds of years), implying enormous computational resources. To tackle this issue, a sequential architecture of a global-regional modelling platform has been developed for the first time and is described in detail in this paper. First of all, the platform is validated for the historical period. It is then used to investigate the climate and in particular, the oceanic circulation, during the Early Holocene. This period was characterised by a large reorganisation of the MTC that strongly affected oxygen supply to the intermediate and deep waters, which ultimately led to an anoxic crisis (called sapropel). Beyond the case study shown here, this platform may be applied to a large number of paleoclimate contexts from the Quaternary to the Pliocene, as long as regional tectonics remain mostly unchanged. For example, the climate responses of the Mediterranean basin during the last interglacial (LIG), the last glacial maximum (LGM) and the Late Pliocene, all present interesting scientific challenges which may be addressed using this numerical platform.

1 Framework of the study

1.1. Introduction

The Mediterranean basin is a key region for the global climate system. It is considered to be a climate “hotspot” (Giorgi, 2006), due to its high sensitivity to global warming. In the past, it has been the seat

36 of important human civilisations, and it continues to play a very important role in international
37 geopolitics with a dense population along its coasts. There is great diversity in the Mediterranean
38 ecosystems, both marine and terrestrial. The Mediterranean region is also rich in paleoclimate records
39 with a variety of proxies. Indeed, this area experienced major changes during the glacial-interglacial
40 cycles (Jost et al., 2005; Ludwig et al., 2018; Ramstein et al., 2007). Another long-term cycle of changes
41 due to high-frequency precession which drastically modified the hydrological patterns of this area
42 (monsoon, sapropels) is also superimposed.

43
44 Due to the peculiarities of both the atmospheric and oceanic circulation in the region, high-quality
45 climate modelling of the Mediterranean region needs to have high spatial resolution (Li et al., 2006).
46 Indeed, the presence of strong gusts of wind in winter are essential to trigger oceanic convection and
47 these can only be correctly represented in high-resolution models. Limited area models (LAM), or
48 regional climate models (RCM), present some advantages in this regard, since they generally demand
49 less computing resources, allowing them to be run at high spatial resolution for a given region. However,
50 their usefulness for paleoclimate purposes is limited because of the lack of adequate lateral boundary
51 conditions to drive the RCMs. The main reason why few comprehensive modelling exercises to explain
52 paleoclimate changes around the Mediterranean have been performed is that the level of computing
53 resources required for high resolution and long simulations is inaccessible. This is especially true in the
54 case of the Mediterranean Thermohaline Circulation (MTC), which has significantly changed in the
55 past, at both centennial and millennial scales.

56
57 Here we describe a modelling suite to define high-resolution atmospheric conditions over the
58 Mediterranean basin from global ESM (Earth System Model) paleoclimate simulations. This
59 atmospheric forcing can then be used to run a highly resolved ocean model (NEMOMED8 1/8°) to
60 accurately simulate ocean dynamics. This tool allows us to achieve a high spatial resolution and
61 equilibrated simulations with a run time of 100 years. The objective of this study is to develop a
62 modelling platform sufficiently comprehensive to conduct paleoclimate studies of the Mediterranean
63 basin. The potential of this platform is illustrated by investigating climate situations from the present
64 period and from the Early Holocene that is supposed to generate sapropel events.

65
66 The sapropel events provide excellent case studies on the impact of global changes on the Mediterranean
67 basin. These periodic events are related to a long period of anoxia of the deep and bottom waters
68 triggered by an enhancement of the African monsoon caused by periodicities of the orbital precession.
69 However, the localisation of the forcing source caused by orbital variability is still a subject of debate.
70 This is especially true for the last sapropel, denoted S1, which occurred during the early Holocene
71 (between 10500 and 6800 ka BP) (De Lange et al., 2008). Reproducing past climate variations over the

72 Mediterranean basin, including the sapropel events, is therefore a challenge for the modelling
73 community.

74

75 The paper is organised as follows: In the first section, we briefly review the different approaches used
76 to simulate the Mediterranean climate and sea conditions, and we also present the concept of the
77 sequential procedure that we propose. Section 2 presents in detail the model architecture we developed.
78 Finally, we present applications with simulations of the historical period (1970-1999) in Section 3 and
79 the Early Holocene (around 9.5 ka) in Section 4.

80 **1.2. Overview of current Mediterranean Sea modelling**

81 The Mediterranean Sea, due to its limited size and its semi-enclosed configuration, has a faster
82 equilibrium response (10^2 years) than the global ocean (10^3 years). Because of this semi-enclosed
83 configuration, there are a few requirements that modelling of the Mediterranean Sea needs to satisfy so
84 that its evolution can be properly represented. High resolution in both the atmospheric forcing and the
85 oceanic configuration is necessary to correctly simulate the convection areas and the associated
86 thermohaline circulation (Lebeaupin Brossier et al., 2011; Li et al., 2006). Depending on the mechanism
87 studied, the resolution of the ocean model used by the research community ranges from $1/4^\circ$ (e.g. for
88 paleo-climatic simulation), to $1/75^\circ$ (for hourly description of the mixed layer, tide-based investigation).
89 The results for oceanic convection are highly dependent on the flux of heat, flux of water, and the wind
90 stress at the air-sea interface especially the seasonal variability and intensity. There are many modelling
91 configurations in the scientific literature making it impossible to provide an exhaustive review of all of
92 them. We can summarise them by presenting the different approaches used to drive the Mediterranean
93 oceanic model, along with their advantages and drawbacks. We underline our new, coherent method,
94 which captures the changes in ocean dynamics in the Mediterranean basin derived from global
95 paleoclimate simulations.

96

97 *Observations and reanalysis*

98 The most common way to simulate the general circulation of the Mediterranean Sea is to run a regional
99 oceanic general circulation model forced by surface fluxes and wind stresses derived from observations
100 and reanalyses. In this way, an oceanic model can be driven by realistic fluxes. In most cases, this implies
101 an observation-based reconstruction of relevant variables with a spatial atmospheric resolution of less
102 than 50 km and a daily temporal resolution, at a minimum, in order to simulate the formation of dense
103 water (Artale, 2002). This approach is adapted to simulate the present-day Mediterranean Sea and to
104 explore the complexity of its sub-basin circulation and water mass formation (Millot and Taupier-
105 Letage, 2005). However, it is not well adapted to the study of past and future climate, partly due to the
106 excessive computing resources needed.

107

108 *Atmospheric model*

109 A second method consists of forcing a regional oceanic model with simulations from an atmospheric
110 model, AGCM (Atmospheric Global Climate Model) or ARCM (Atmospheric Regional Climate
111 Model). Since the AGCM resolution (typically 100 to 300 km horizontally) is coarse, statistical and/or
112 dynamical downscaling is usually needed, especially for wind-stress so that the ORCM (Ocean Regional
113 Circulation Model) can be correctly forced (Béranger et al., 2010). Currently, dynamical downscaling
114 with ARCM is the preferred option because it generally improves simulations of the climate in the
115 Mediterranean region and especially of the hydrological cycle (Li et al., 2012).

116

117 This configuration is broadly used to assess anthropogenic climate changes (Adloff et al., 2015; Macias
118 et al., 2015; Somot et al., 2006). In these studies, the Mediterranean Sea simulations are generally driven
119 by the outputs of an ARCM, which is, in turn, driven by the GCM or observation-based reanalysis. It
120 should be noted that biases in oceanic variables can be reduced through constant flux correction (Somot
121 et al., 2006). This configuration is suitable for high-resolution simulation of the past Mediterranean Sea
122 (Mikolajewicz, 2011 for the LGM; Adloff et al., 2011 for the Early Holocene among others).

123

124 *Regional coupled model*

125 Although the majority of the Mediterranean Sea models are ocean-alone models, some of them use a
126 coupled configuration between the Mediterranean Sea and the atmosphere. Such a coupled configuration
127 generally improves the simulation of the air-sea fluxes, including their annual cycle (de Zolt et al., 2003),
128 but may show climate drifts in key parameters such as the SST. Regional coupled models are now
129 emerging as a tool in Mediterranean climate modelling (Artale et al., 2010; Dell'Aquila et al., 2012;
130 Drobniski et al., 2012; Sevault et al., 2014; Somot et al., 2008). However, this full-coupling
131 configuration is currently not possible for high-resolution paleoclimate issues requiring long simulation
132 for hundreds or thousands of years.

133

134 *Importance of boundary conditions*

135 The boundary conditions applied to the Mediterranean Sea domain, in particular, the exchanges of water,
136 salt and heat with the Atlantic Ocean through the Strait of Gibraltar modulate significantly the
137 Mediterranean circulation (Adloff et al., 2015). This is especially true at the millennial scale where
138 deglaciation episodes and fluctuations of the AMOC (Atlantic Meridional Overturning Circulation) and
139 the Mediterranean Sea affect each other (Swingedouw et al., 2019). The level of discharge from the
140 main rivers is also crucial as is illustrated by the sapropel episodes, where an increase in freshwater
141 input drastically slowed down the MTC. Most of current models impose prescribed (observed when
142 possible) conditions in the near Atlantic zone, including temperature and salinity. The same
143 methodology can be used to prescribe river discharges. However, it must be acknowledged that

144 determining inputs from rivers into the Mediterranean Sea, either of water or other materials, still
145 presents serious challenges for modelling.

146 **1.3. Concepts for a sequential procedure to perform global-to-regional modelling**

147 In this paper, a new architecture for high-resolution modelling of the climate of the Mediterranean basin
148 for past, present and future conditions is proposed. This architecture is based on a method that provides
149 as much compatibility as possible amongst the models used and high consistency with data~~This~~
150 ~~architecture is based on a method as much consistency among the models as possible and high~~
151 ~~congruency with data.~~

153 *Step 1: Global climate*

154 Our goal is to simulate different climate conditions for the Mediterranean basin. The first step of any
155 relevant procedure should be to simulate the global climate conditions from which the simulation of the
156 regional climate is driven. These may be already available in simulations from previous PMIP exercises
157 for various periods (e.g. mid-Holocene, Last Glacial Maximum, Last Interglacial and mid-Pliocene) as
158 well as for different sapropel events and interglacials (e.g. MIS11, MIS13 and MIS19). However, this
159 is not always possible due to the large volume of high-frequency 3-D atmospheric circulation variables
160 involved. An alternative approach, used in some regional climate simulations (Chen et al., 2011;
161 Goubanova and Li, 2007; Krinner et al., 2014), consists of using an AGCM (either an independent one
162 or the same one used for the global climate simulation) run with appropriate values for global Sea
163 Surface Temperature (SST) and Sea Ice cover (SIC), derived from PMIP global simulations. SST is
164 crucial to determine atmospheric features and responses, while SIC plays a key role in determining the
165 global albedo. Monthly SST and SIC are necessary and sufficient to drive an AGCM. They can be
166 acquired from global climate simulations or through a bias-correction procedure.

168 *Step 2: Regional climate*

169 After running an AGCM, regional climate can be now reproduced with an ARCM nested into the high-
170 frequency outputs from the AGCM. Of course, the ARCM can be run in parallel to the AGCM, or with
171 a small time delay. Thus, we avoid a large accumulation of intermediate information between the AGCM
172 and the ARCM. In our study, we assume that there would be no feedback from the regional scale to the
173 global scale, so only a “one-way” transfer of information (from global to regional) is considered. In our
174 case, the ARCM is a strongly zoomed-in version of the AGCM and is also driven by monthly SST and
175 SIC values, as used for AGCM. The higher resolution of the ARCM allows the synoptic variability and
176 seasonality of the Mediterranean region to be depicted so that a realistic wind pattern and hydrological
177 cycle may be reproduced. This approach provides a general framework for use in many different

178 paleoclimate periods from the Pliocene to the Pleistocene, as long as the basin tectonics remain
179 unchanged.

180

181 *Step 3: Mediterranean Sea Circulation*

182 Daily air-sea fluxes and wind stress provided by the ARCM are used as surface boundary conditions to
183 drive the ORCM to investigate the oceanic dynamics of the Mediterranean. It is reasonable to assume
184 that the boundary conditions of these air-sea fluxes represent the long-term trends of the oceanic
185 dynamics. Rivers may be considered interactive or not depending on the investigative objectives: runoff
186 can be prescribed from climatology or obtained from the hydrological component of the surface model.
187 Again, we highlight that our architecture does not include any feedback, between either the regional
188 ocean and the regional atmosphere, or the regional ocean and the global ocean. This configuration means
189 that we can avoid dealing with certain issues, for example, the influence of the Mediterranean Outflow
190 Water on the North Atlantic Ocean but is well adapted to provide consistent river runoff associated with
191 changes in continental precipitation.

192 **2 Model architecture**

193 An ensemble of modelling tools that includes two atmospheric models and a regional oceanic model is
194 used. Figure 1 summarises the configuration and shows the experimental flowchart.

195 **2.1. The atmospheric models (AGCM and ARCM)**

196 LMDZ4 (Hourdin et al., 2006; Li, 1999) is the atmospheric general circulation model developed and
197 maintained by IPSL (Institut Pierre Simon Laplace). It has been widely used in previous phases of CMIP
198 and PMIP projects. The resolution of the model is variable. Its global version used here (referred to as
199 LMDZ4-global) is 3.75° in longitude and 2.5° in latitude with 19 layers in the vertical. It provides the
200 boundary conditions to drive LMDZ4-regional. LMDZ4-regional (Li et al., 2012) is a regionally-
201 oriented version of LMDZ4 with the same physics and same vertical discretisation, dedicated to the
202 Mediterranean region. The zoomed-in model covers an effective domain of 13°W to 43°E and 24°N to
203 56°N with a horizontal resolution of about 30 km inside the zoom. The rest of the globe outside this
204 domain is considered to be the buffer-zone for LMDZ4-regional where a relaxation operation is
205 performed to nudge the model with variables from the AGCM, at a 2-hour frequency. The resolution of
206 LMDZ4-regional decreases rapidly outside its effective domain. In both LMDZ4-global and LMDZ4-
207 regional, land-surface processes, including the hydrological cycle, are taken into account through a full
208 coupling with the surface model, ORCHIDEE (Krinner et al., 2005).

209 2.2 The regional oceanic model (ORCM)

210 NEMOMED8 (Beuvier et al., 2010; Herrmann et al., 2010) is the regional Mediterranean configuration
211 of the NEMO oceanic modelling platform (Madec, 2008). The horizontal domain includes the
212 Mediterranean Sea and the nearby Atlantic Ocean which serves as a buffer zone (from 11°W to 7.5°W).
213 The horizontal resolution is $1/8^\circ$ in longitude and $1/8^\circ \cos\varphi$ in latitude, i.e. 9km to 12km from the north
214 to the south. The model has 43 layers of inhomogeneous thickness (from 7 m at the surface to 200 m in
215 the depths) in the vertical. River discharges are accounted for as freshwater fluxes in the grids
216 corresponding to the river mouths. A dataset of climatological river discharges ~~is~~ was proposed by
217 default to cover the entire Mediterranean draining basin with 33 river mouths. It is of course switched
218 off when rivers are interactive in the platform. The interactive calculation of freshwater discharges from
219 rivers by the land-surface model, ORCHIDEE, includes 192 river mouths ~~thatt~~ cover the Mediterranean
220 draining basin. The Black Sea, not included in NEMOMED8, counts as a river dumping freshwater into
221 the Aegean. The Black Sea fresh water assumption comes from NEMOMED modeling community that
222 consider it as a yearly source of freshwater. The deposit rate is calculated based on total runoff into the
223 Black Sea, plus the net budget of precipitation (P) minus evaporation (E) over the Black Sea.

224

225 When the oceanic model NEMO is used alone, with prescribed surface fluxes, it is indispensable to
226 implement a restoring term with a constant coefficient of $40 \text{ W}\cdot\text{m}^{-2}\cdot\text{K}^{-1}$ (as defined in Barnier et al. 1995)
227 . This is a standard procedure for NEMO to prevent eventual run-away cases. In our modelling chain,
228 the target temperature for the restoration is the surface air temperature from the regional atmospheric
229 model LMDZ4-regional.

230 2.3 Modelling Sequence

231 As shown in Fig. 1, the first step in our modelling chain is to obtain SST and SIC values from an Earth
232 System Model simulation able to reproduce global climate (for the past, present or future). We can
233 reasonably hypothesise that major global climate information can transit from global SST and SIC. This
234 hypothesis was deemed legitimate for climate downscaling purposes for Antarctic and Africa, in Krinner
235 et al. (2014) and Hernández-Díaz et al. (2017) respectively. In the present work we use IPSL-CM5A
236 (Dufresne et al., 2013) to extract relevant SST and SIC values to drive the AGCM (LMDZ4-global) and
237 the ARCM (LMDZ4-regional). The next step is to run the two atmospheric models, LMDZ4-global and
238 LMDZ4-regional, in the usual way as proposed by the AMIP community. This is the most expensive
239 step, as atmospheric models are the most demanding in terms of computing resources. Fortunately, it is
240 not necessary to run them for a long time as the atmosphere reaches equilibrium quickly. We applied 30
241 years of simulation to both models. We consider this duration to be long enough to depict climate
242 variability for the simulation of past events. The AGCM nudges the ARCM in the conventional way of
243 one-way nesting for temperature, humidity, meridional and zonal wind every two hours. The nudging is

244 done using an exponential relaxation procedure with a timescale of half an hour outside the zoom and
245 10 days inside the zoom. Table S2 in the SOM summarises the forcings used, especially the orbital
246 forcing and atmospheric CO₂.

247 The necessary variables (surface air temperature, wind stress, P-E over the sea, heat fluxes) are provided
248 by ARCM to NEMOMED8 (ORCM) at daily frequency. The salinity and temperature conditions are
249 provided in three dimensions in the Atlantic buffer zone, near the Gibraltar Strait, and updated every
250 month. River runoff, updated every month, depends on the configuration used (prescribed climatological
251 rivers, or interactive rivers). Table S3 in SOM details these boundary conditions.

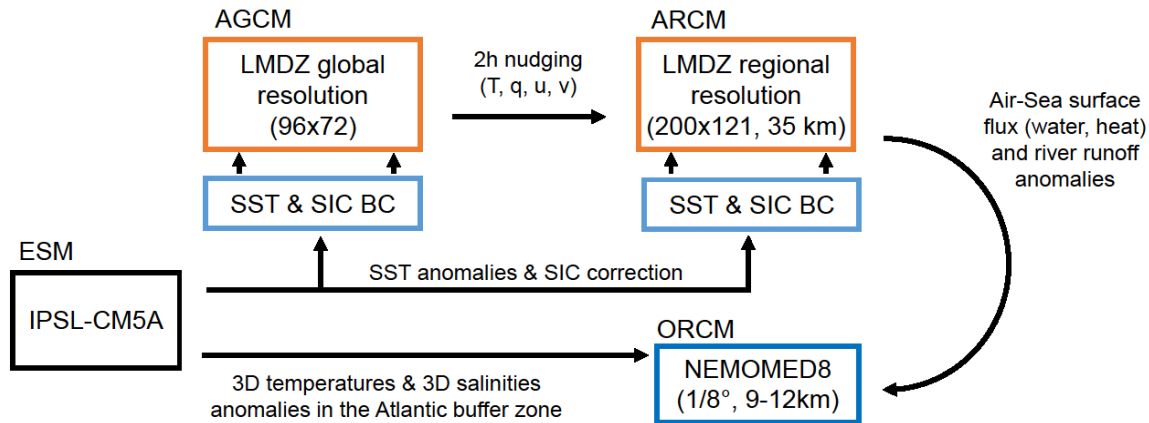
252 It is worthy to mention the work of Mikolajewicz (2011) who used a similar modelling chain (from a
253 coarse-resolution earth system model to a high-resolution regional oceanic model) to simulate the
254 Mediterranean Sea climate during the last glacial maximum. However, Mikolajewicz (2011) used only
255 an AGCM (ECHAM5) as the intermediate step. In our case, we found that the use of ARCM was
256 indispensable to produce high-quality forcing to correctly simulate the oceanic convection in
257 NEMOMED8.

258 **2.4 Bias correction**

259 The sequential modelling chain, despite the lack of interactivity and feedback at interfaces, allows for
260 error removal and bias correction at each step of the methodology. This adjustment is sometimes crucial,
261 especially when model outputs need to be of very high quality to be incorporated into impact studies.
262 This concept was further described in Krinner et al. (2019), as illustrated in Fig. 16 of their paper.
263 Therefore, to enhance our confidence in the realism of the simulation results, bias-correction may be
264 introduced when necessary. The correction method used in the present work generally follows the
265 conventional procedure, which is based on the difference between the model outputs for present day
266 simulations and actual observations. Biases corrected in this way, theoretically only valid for the
267 historical simulation (named HIST hereafter), are assumed to remain unchanged for past and future
268 simulation scenarios. However, the transferability between past and future periods is questionable. There
269 is no guarantee that the model error for one period is the same for other periods, even though the model
270 physics may be the same. In addition, paleodata are often rare and incomplete, and so, are unsuitable for
271 evaluation and correction of model errors. The most reliable basis is that established for the present day.
272 The reader can find a full description of the bias corrections and their eventual use in our applications
273 in the supplementary online material, “Text S2: Bias correction”.

274

275



276

277

278 **Figure 1: Flowchart of the modelling chain including the four main components generally**
 279 **represented by ESM, AGCM, ARCM and ORCM, respectively, and actually implemented in our**
 280 **platform by IPSL-CM5A, LMDZ-global, LMDZ-regional and NEMOMED8. BC: boundary**
 281 **condition, u: zonal wind, v: meridional wind, q: specific humidity, T: temperature, S: salinity,**
 282 **SST: sea surface temperature, SIC: sea-ice concentration.**

283 3 Validation of the modelling chain for present-day climate 1970-1999

284 In this section, the capacity of the model to reproduce the climate of the recent past is evaluated, in
 285 particular, its ability to simulate sea surface characteristics as well as the Mixed Layer Depth (MLD)
 286 and oceanic convection patterns as these are key elements to reproduce the evolution of the
 287 Mediterranean Sea in past climate conditions.

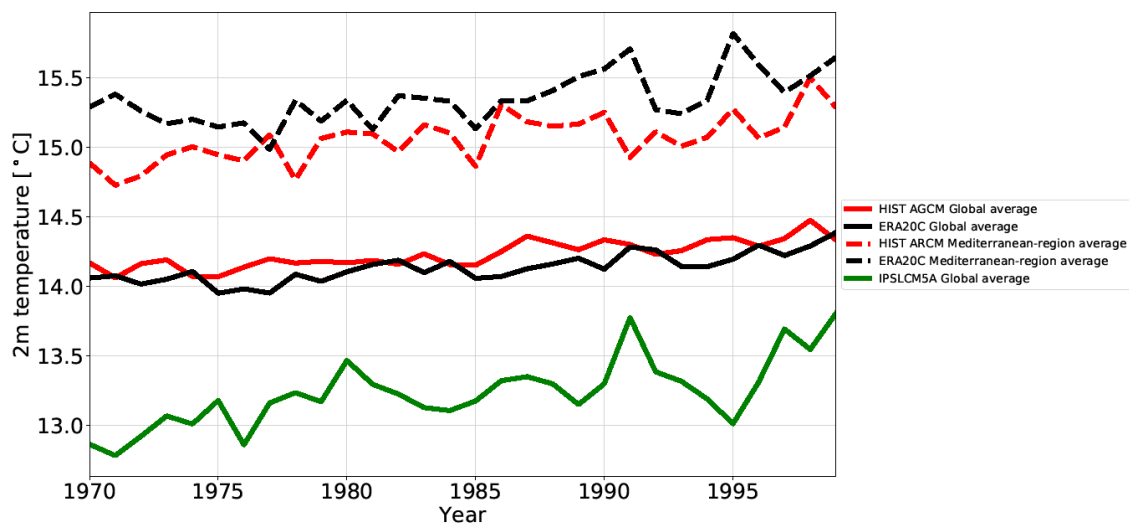
288 3.1 Experimental design

289 For the HIST experiment, SST and SIC observations (ERA-Interim, Dee et al., 2011) are used to force
 290 the AGCM. River runoff is from the climatology of Ludwig et al., (2009). Monthly mean climatological
 291 sea temperatures and salinities (World Ocean Atlas database from Locarnini et al., 2013, Zweng et al.,
 292 2013) are used for the Atlantic boundary zone. HIST atmospheric simulations for both global and
 293 regional simulations have a duration of 30 years. The length of the HIST oceanic simulation is also 30
 294 years, but obtained after a 150-year spin-up. The forcings for each experiment are detailed in “Tables
 295 S2 and S3” in the supplementary online material. Spin-up phases for each simulation are also shown
 296 from “Figure S4” to “Figure S8” for the overturning stream function and the index of stratification.

297 **3.2 Evolution of temperatures**

298 Figure 2 depicts the temporal evolution, between 1970 and 1999, of annual mean surface air
 299 temperatures at two metres in the atmospheric simulations (global and regional) compared to
 300 observations for the whole globe and over the Mediterranean region. The two models reproduce a range
 301 of temperatures similar to the observations, with the Mediterranean temperatures warmer than the global
 302 temperatures. The global simulation (continued red curve in Fig. 2), after SST bias correction, is very
 303 close to the observation (continued black curve), with a tremendous improvement compared to
 304 IPSLCM5A (green curve in Figure 2)~~The global simulation, after SST bias correction, ranged with the~~
 305 ~~observation, compared to IPSLCM5A (Figure 2).~~ The regional model reproduces the warming trend and
 306 aspects of the interannual variability ~~which are quite~~ close to observations, but with a mean cold shift of
 307 about -0.6°C.

308
309
310



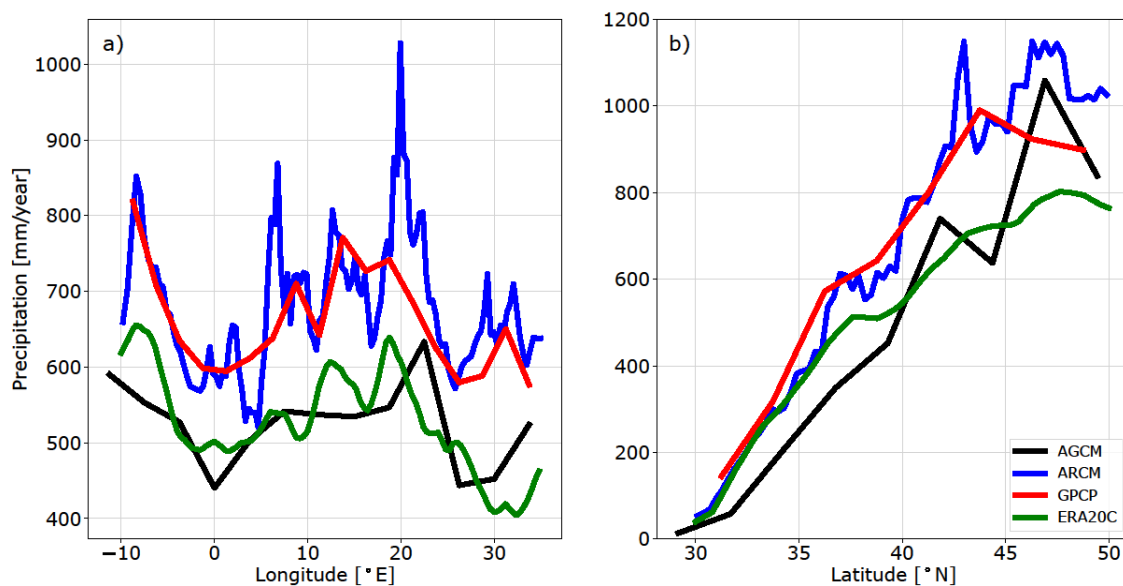
311
 312 **Figure 2: Time series of annual mean surface air temperatures at 2 m in HIST (red) and ERA20C**
 313 **(black, ref: Stickler et al., 2014) and IPSLCM5A (green) for global average (solid lines) and**
 314 **Mediterranean-region (10°W- 35°E, 20°N-50°N) average (dashed lines).**

315 ~~**Figure 2: Time series of annual mean surface air temperatures at 2 m in HIST (red) and ERA20C**~~
 316 ~~**(black, ref: Stickler et al., 2014) and IPSLCM5A (green) for global average (solid lines) and**~~
 317 ~~**Mediterranean-region (ocean and continent) average (dashed lines).**~~

318 **3.3 Precipitation and freshwater budget**

319 Figure 3 a and b show the average annual precipitation for 1970-1999 in HIST over the Mediterranean
 320 region and the differences with observations. The main features of the distribution of precipitation over
 321 the Mediterranean region are simulated, in particular the distinct contrast between the very low

322 precipitation in the southern region and higher precipitation in the north. The ARCM tends to generate
 323 higher precipitation than the AGCM due to the resolution refinement. Compared to observation, AGCM
 324 is closer to ERA20C (Stickler et al., 2014), whereas ARCM is closer to GPCP data (Adler et al., 2018).
 325 However, the regional model still overestimates the amount of precipitation, especially at 42°N, from
 326 45° to 50° N, at 8°E and 20°E. It corresponds to most of Europe, especially over the Alps, the Pyrenees,
 327 the Balkans and other mountainous regions. The freshwater budget over the Mediterranean Sea from
 328 observations (a synthesis from Sanchez-Gomez et al., 2011 and from other sources) and in the various
 329 simulations conducted in this study are summed up in Table 1. The simulated continental precipitation
 330 is overestimated, but both the precipitation and evaporation over the Mediterranean Sea in HIST are
 331 very close to the observations, with 10 mm.yr⁻¹ of oceanic precipitation difference between HIST and
 332 the mean observation value (by taking the upper and the lower value), and 18 mm.yr⁻¹ for the oceanic
 333 evaporation. The two other simulations included in Table 1, PICTRL and EHOL, are those designed to
 334 investigates the Early Holocene climate (see Section 4)Two other simulations, PICTRL and EHOL, are
 335 those designed in Section 4 to investigate the Early Holocene climate.
 336



337
 338
 339 **Figure 3: Annual mean precipitation, a) meridionally averaged (30 to 50°N), b) zonally averaged**
 340 **(-10 to 35°E), in the historical simulations with AGCM (LMDZ-global) and ARCM (LMDZ-**
 341 **regional). Observation comes from GPCP (Global Precipitation Climatology Project, 1979 to**
 342 **1999, blue line, ref: Adler et al., 2018). and ERA20C (green line, ref: Stickler et al., 2014).**
 343

Dataset or experiment	E	P	R	B	E - P - R - B

OBS	1096-1136	256-595	102-142	73-121	238-705
HIST	1106	443	74	104	485
PICTRL	1031	451	98	104	378
EHOL	1094	460	225	104	305

344 **Table 1: The Mediterranean Sea freshwater budget, expressed as $\text{mm}\cdot\text{year}^{-1}$ for the whole water**
345 **area (about 2.5 million of km^2). E, evaporation, P, precipitation, R, river runoff, B, Black Sea**
346 **discharge into the Mediterranean Sea. OBS is a summary from Sanchez-Gomez et al., (2011) for**
347 **P, E and P-E, from Ludwig et al., (2009) for R, from Lacombe and Tchernia, (1972), Stanev et al.,**
348 **(2000) and Kourafalou and Barbopoulos, (2003) for B. River discharges in HIST are from the**
349 **climatology of Ludwig et al., (2009). PICTRL uses the Nile of its pre-industrial (pre-damming)**
350 **value, $2930 \text{ m}^3\cdot\text{s}^{-1}$, annually (Rivdis database, Vorosmarty et al., 1998). River discharges in EHOL**
351 **are deduced from the difference between EHOL and PICTRL.**

352

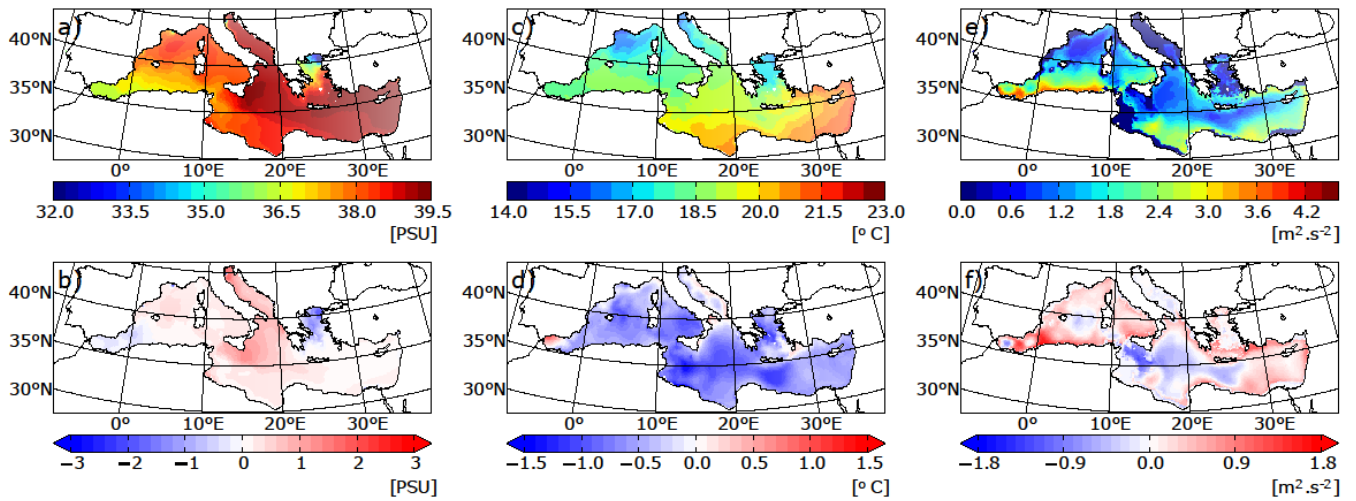
353 **3.4 Mediterranean Sea surface characteristics**

354 Figure 4 displays the temperatures and salinities of the Mediterranean Sea simulated in HIST and the
355 deviations from observations. The model is able to capture the main characteristics of the pronounced
356 west-east gradient of SSS in the Mediterranean Sea (Figure 4 a). Values are within the range of
357 observations (mean bias = 0.32 PSU, error = 0.37 PSU, table 2). In the simulation, the Aegean Sea is
358 not salty enough (about -1.5 PSU) and the Adriatic/Ionian Sea is too salty (+1 PSU).

359 The model reproduced the northwest to southeast temperature gradient, as shown in Figure 4b. However,
360 the model shows a general cold bias (from -0.5 to -1.5 °C) over the entire Mediterranean (Figure 4e),
361 due to the cold bias already observed for the air temperature at 2m in the regional atmospheric forcing
362 (cf Figure 2).

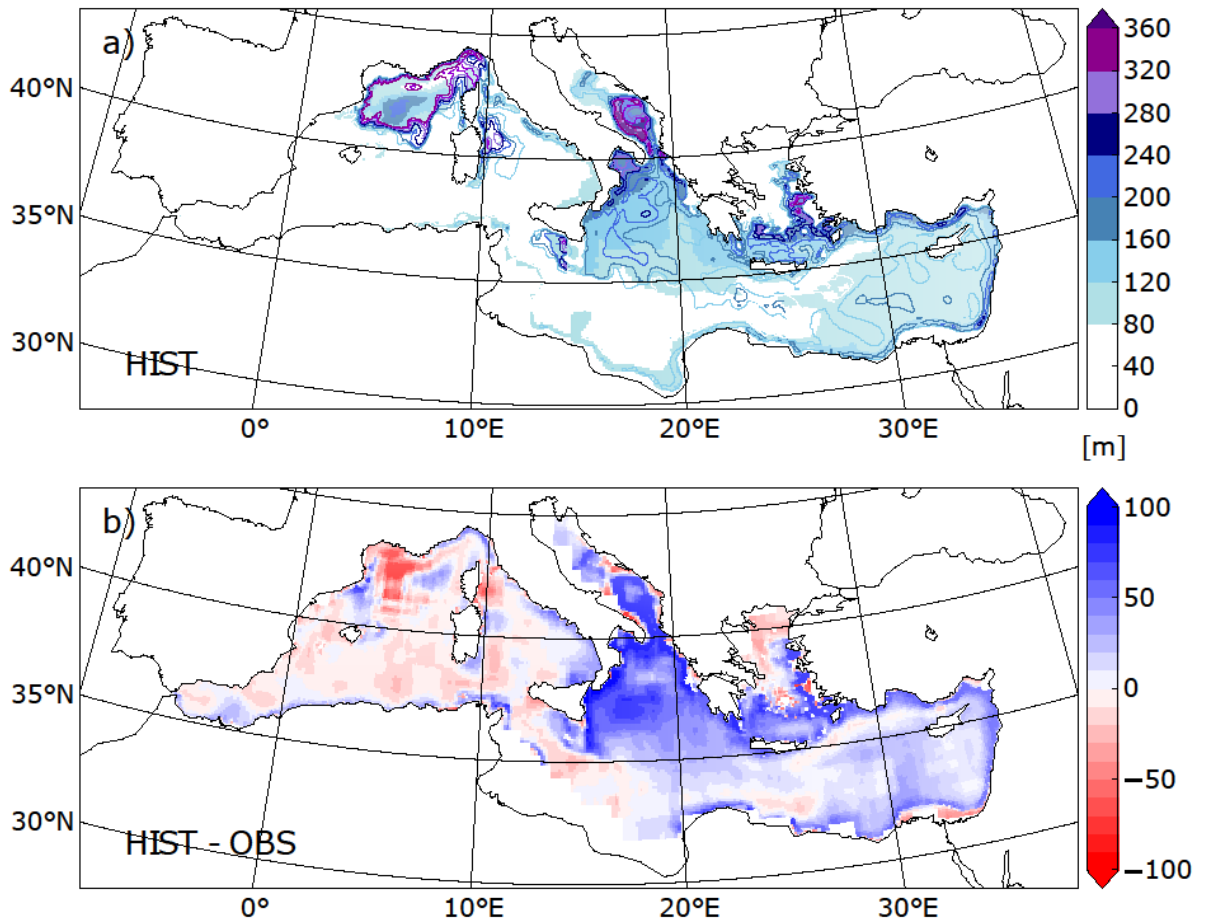
363

364



365
 366
 367
 368
 369
 370
 371

Figure 4: Annual mean sea-surface salinity (left panels, SSS in PSU), sea-surface temperature (middle panels, SST in °C) and index of water column stratification (right panels, winter IS in $m^2.s^{-2}$) simulated in HIST (top panels) and the HIST deviation (model - obs) from the observation-based MEDATLAS data (averaged over the entire simulation).



372

373 **Figure 5: a) Mixed layer depth simulated in HIST (panel a, in m) and as deviation (b) of HIST**
 374 **from observations of Houpert et al., (2015) averaged over the entire simulation for JFM (January**
 375 **February March). Contour lines in the upper panel a) represents the maximum of MLD**
 376 **throughout the HIST simulation.**
 377

	SST (°C)	SSS (PSU)	IS (m ² .s ⁻²)
Mean bias (model – obs)	-0.64	0.32	0.91
RMS error	0.45	0.37	0.29

378
 379 **Table 2: Mean biases of sea surface temperature (SST), sea surface salinity (SSS) and index of**
 380 **stratification (IS) in the HIST simulation, expressed as the deviation from observations**
 381 **(MEDATLAS-II), and associated root mean square errors.**

382 3.4 Mediterranean Thermohaline circulation

383 Here, the general characteristics of the simulated thermohaline circulation is evaluated in regions where
 384 deep and intermediate water formation occurs. Figure 4c displays the stratification index (IS¹) for HIST.
 385 IS is a vertical integration of the Brunt-Vaisala frequency. A lower IS implies that convection is more
 386 likely. The range of IS biases (Figure 4f), is from -1 to 1 m².s⁻² (mean bias = 0.91 m².s⁻², error = 0.29
 387 m².s⁻²). The model satisfactorily reproduces the convection in known intermediate and deep-water
 388 formation areas, namely the Gulf of Lions, the Adriatic Sea, the Ionian Sea, the Aegean Sea and the
 389 North Levantine.

390
 391 Comparison with observations of the mixed-layer depth (Houpert et al., 2015) confirms that the model
 392 reproduces realistic intermediate and deep-water formation patterns, with a thicker MLD in the eastern
 393 basin, due to salty condition (Figure 4a and e), and a shallower MLD in the Gulf of Lions (figure 5b).
 394

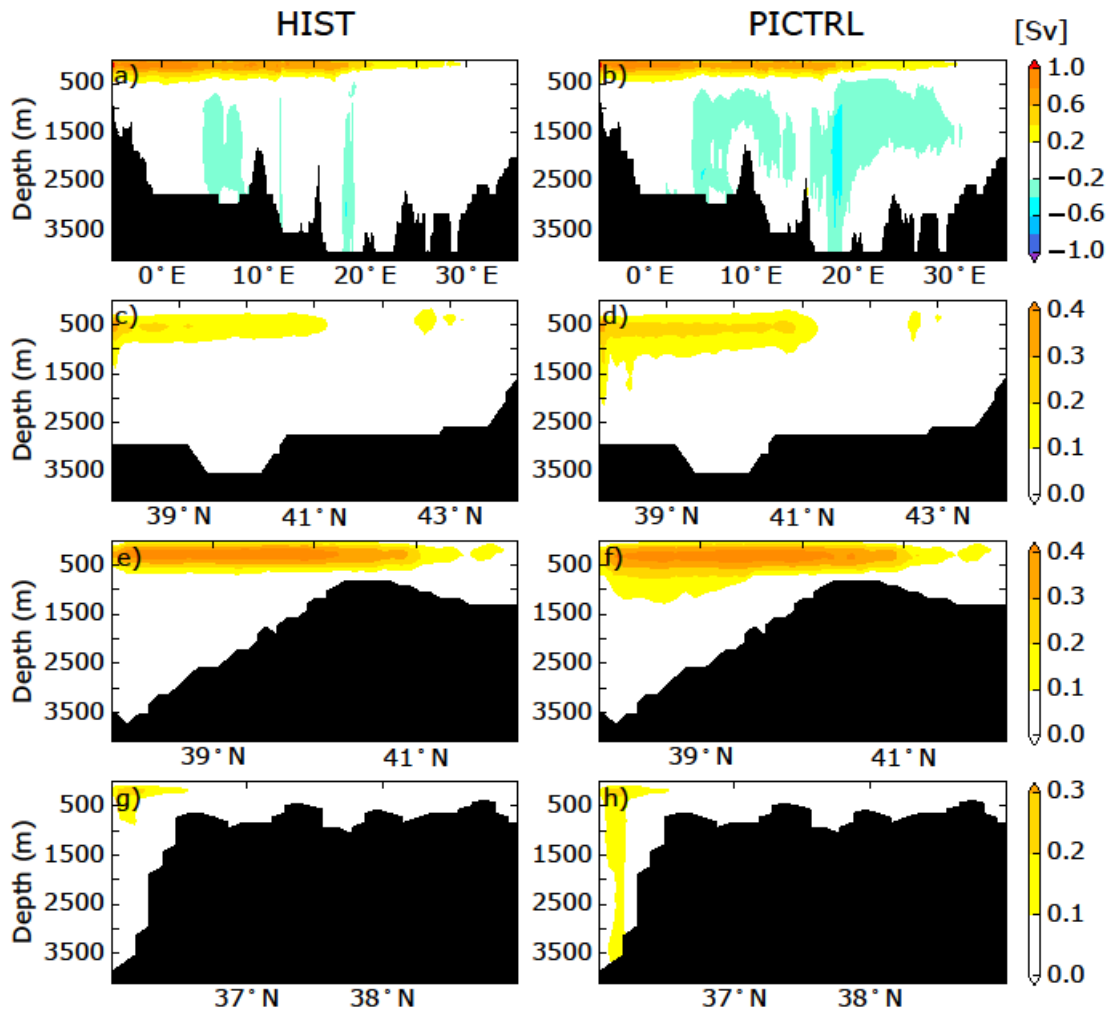
395 The simulated Mediterranean overturning circulation is analysed (figure 6). The Zonal Overturning
 396 stream Function (ZOF²) in figure 6a depicts the surface and intermediate circulation and the

¹ $IS(x, y, h) = \int_0^h N^2(x, y) z dz$. N^2 is the Brunt-Väisälä frequency. IS is calculated at each model grid (x, y) for a given depth h (set as the bottom of the sea, or as 1000 m when the depth is greater than 1000 m).

² $ZOF(x, z) = \int_h^z \int_{y_s}^{y_n} u(x, y, z) dy dz$. u is the zonal currents, h is the depth of the bottom, y_n and y_s are the north and south coordinates respectively.

397 intermediate/deep circulation. The surface current from the Strait of Gibraltar flows up to 30°E and back
398 to the Atlantic Ocean in the intermediate layers, through the Levantine Intermediate Water (LIW)
399 outflow. Figure 6 c, e, and g represents the Meridional Overturning stream Function (MOF³) in the Gulf
400 of Lions, the Adriatic Sea and the Aegean Sea, respectively. The surface cell in the longitude-depth plan
401 is comparable to previous studies done with the same regional oceanic model, but with different forcings
402 (Adloff et al., 2015; Somot et al., 2006): the mean strength of the surface cell ranges from 0.8 to 1.0 Sv,
403 and the longitudinal extension is from 5°W to 30°E. The simulated intermediate and deep cells are
404 recognized in existing studies as having different characteristics. Our simulated pattern is very close to
405 a similar historical run in Adloff et al., (2015), but is weaker than a historical run in Somot et al., (2006),
406 and a second historical configuration (with refined air-sea flux) in Adloff et al., (2015). The ZOF in
407 HIST depicted in figure 6 HIST is consistent with the reanalyses (1987-2013) of Pinardi et al. (2019)
408 over the Western basin, but shows a weaker Eastern deep cell compared to the reconstruction.
409

³ $MOF(y, z) = \int_h^z \int_{x_e}^{x_w} v(x, y, z) dx dz$. v is the meridional currents, h is the depth of the bottom, x_w and x_e are the west and east coordinates respectively.



410

411 **Figure 6: a, b, Zonal Overturning stream-Function (ZOF, first row, panels a, and b) integrated**
 412 **from north to south and shown as a longitude-depth section for the whole Mediterranean Sea, for**
 413 **HIST, and PICTRL simulations (from top to bottom), respectively. Other panels show Meridional**
 414 **Overturning stream-Function (MOF) shown as a latitude-depth section, integrated west/east for**
 415 **the Gulf of Lion (second row c and d, longitudinal extent: 4.5° to 8°E), the Adriatic/Ionian Sea**
 416 **(third row e and f, 12° to 21°E), and the Aegean Sea (fourth row g and h, 24° to 28°E) averaged**
 417 **over the entire simulation for HIST and over the last 30 years of simulation for PICTRL.**

418 3.5 Summary of Validation

419 Validation of our platform was based on the historical period from 1970 to 1999. after bias correction of
 420 global SST, the 2-m surface air temperature in the HIST global simulation is comparable to the
 421 observational counterpart. However, the simulated surface air temperature within the regional model is

422 ~~colder (as shown in Figure2), which implies SST cold biases for the Mediterranean Sea~~Validation of
423 ~~our platform was based on the historical period, 1970 to 1999. The atmospheric simulation is acceptable~~
424 ~~compared with observations for the air temperature at 2m at both global and regional scales.~~The
425 simulated precipitation from the atmospheric models produces a signal that has the same range of
426 variability as the observations~~ranges with the observation~~, but there is significant overestimation of
427 precipitation over the mountainous area and over the land surrounding the Mediterranean Sea. However,
428 the freshwater budget over the sea is close to observations for both evaporation and precipitation. The
429 areas of intermediate and deep convection produced by the model are realistic, and the simulation of the
430 thermohaline circulation is well captured by the oceanic model and in the range of the state-of-the-art
431 existing Mediterranean regional models (compared to the simulations of Adloff et al., 2015 and Somot
432 et al., 2006 for instance) and reanalysis as well (Pinardi et al., 2019). These features inspire confidence
433 in our modelling platform for the investigations of past climate.

434 **4 Application of the modelling chain to the Early Holocene**

435 In this section, results obtained when our sequential modelling chain is applied in a paleoclimate context
436 are presented, which was our initial motivation for developing this modelling tool. We chose to test the
437 performance of our tool on the Early Holocene, a period marked by significant changes in climate and
438 ocean dynamics over the Mediterranean basin, when the last sapropel event, S1, occurred in the
439 Mediterranean Sea. Our experimental design relies on the comparison of two simulations: the Early
440 Holocene (EHOL) with PICTRL based on pre-industrial conditions, the latter acting as a reference.

441 **4.1 Experimental design**

442 As indicated in the general flowchart of our modelling platform, global SST and SIC are required to
443 initiate our sequential modelling. The basic assumption is that the climate change signal can be
444 reconstructed from global SST and SIC, an accepted practice within the climate modelling community.
445 In this study, two existing long-term coupled simulations from IPSL-CM5A is used, one covering the
446 pre-industrial period and the other covering the Early Holocene (around 9.5 ka). Taking the last 100
447 years of each simulation, a climatological SST and SIC is constructed. After conducting bias-correction,
448 these outputs from IPSL-CM5A are then used to drive the AGCM (LMDZ-global) and the ARCM
449 (LMDZ-regional) in a further step. The duration of the PICTRL and EHOL atmospheric simulations is
450 30 years (both global and regional models).

451
452 Oceanic temperature and salinity in the Atlantic buffer-zone, as well as freshwater discharges from
453 Mediterranean rivers, are all bias-corrected for NEMOMED8, as described in the general methodology.
454 However, it needs to be pointed out that the reference point for the Nile river discharge is not modern
455 observations but is set at pre-industrial values ($2930 \text{ m}^3 \cdot \text{s}^{-1}$ for annual mean, Vorosmarty et al., 1998)

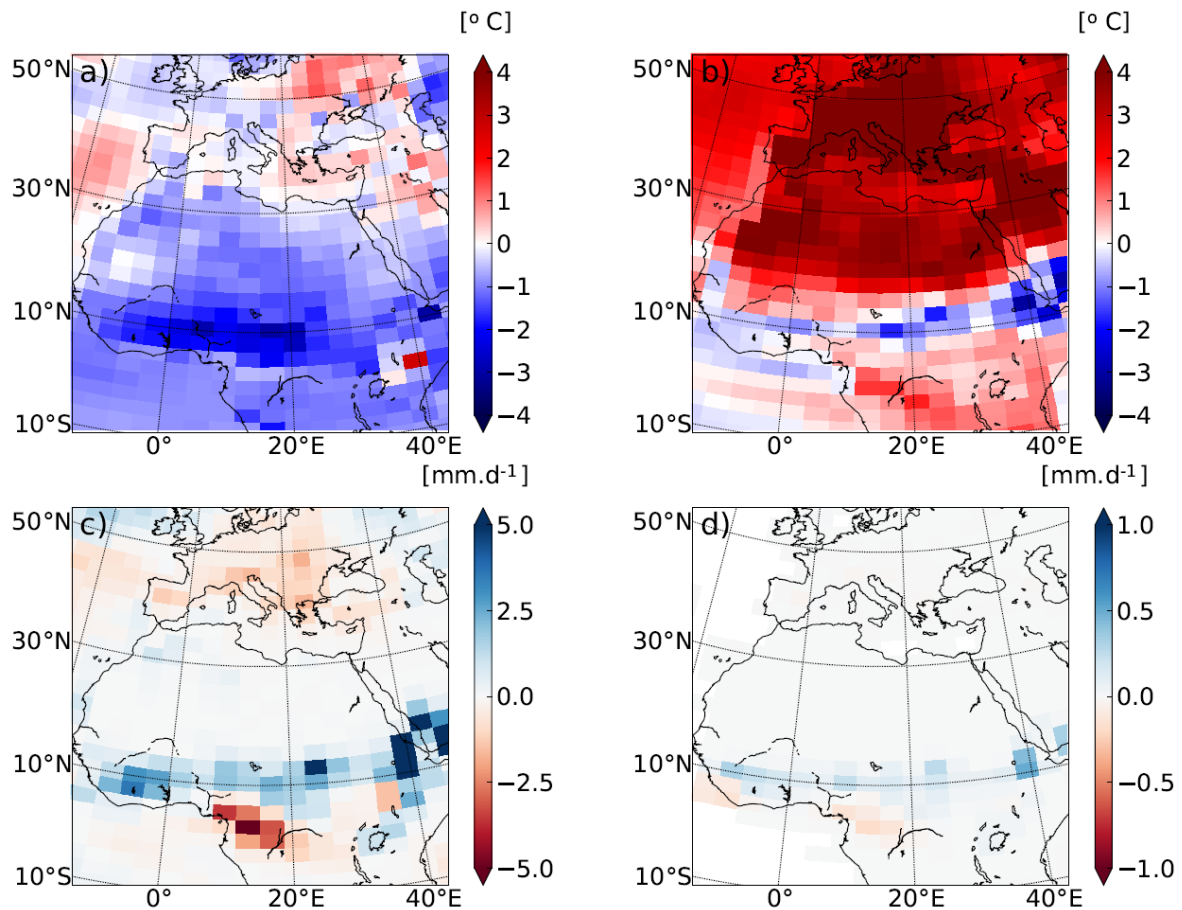
456 corresponding to a period before construction of the Aswan dam. For this part, the water budget over
457 the Black Sea is calculated from the ARCM output. The oceanic simulation is 90 years for EHOL and
458 30 years for PICTRL, performed after a 200-year spin-up of PICTRL.

459 **4.2 Climate features depicted in LMDZ-global (AGCM)**

460 Because Early Holocene simulations are mainly driven by insolation forcing, an important feature is the
461 model response to seasonal temperatures. Figure 7 shows the difference between EHOL and PICTRL,
462 as reproduced in the AGCM, LMDZ-global, for the summer/winter temperature, JJAS precipitation and
463 JAS surface runoff. The atmospheric model imprints a stronger seasonality due to the increased Early
464 Holocene summer insolation. Warmer summer temperatures over Europe and North Africa (+ 6 °C,
465 figure 7b) and lower winter temperatures over Africa (-2 °C, figure 7a) reflect this feature. Variations
466 of the precession also trigger an enhancement of the African Monsoon (+ 10 mm.day⁻¹ over the Ethiopian
467 region, figure 7c). The main consequence of this increase in precipitation is an enhanced surface runoff
468 over the Ethiopian region. This hydrological state is similar to the African Humid Period caused by the
469 enhanced African Monsoon and the resultant increase in surface runoff, as shown in Rossignol-Strick et
470 al. (1982).

471

472 Our results are similar to those of previous modelling exercises for the Early- and Mid-Holocene (e.g.
473 Adloff et al., 2011; Bosmans et al., 2012; Braconnot et al., 2007; Marzin and Braconnot, 2009). They
474 are also consistent with various reconstructions of mid-Holocene precipitation (Harrison et al., 2014).
475 A detailed comparison can be made with the Early Holocene simulation reported in Marzin and
476 Braconnot (2009) which used for their experiment the same orbital parameters and the same atmospheric
477 model as EHOL. However, their model was coupled to an oceanic model, while an atmospheric model
478 and prescribed SST and SIC as boundary conditions are used in this study. Generally speaking, our
479 results for both surface air temperature and precipitation are very similar to those of Marzin and
480 Braconnot (2009), attesting to the validity of our approach using a simple atmospheric model
481 constrained by boundary conditions. In the ensemble of PMIP simulations, available for the Early
482 Holocene and mid-Holocene, there are some robust outputs for the climate response to orbital forcing
483 but there are also some weaknesses common to most of the models (Braconnot et al., 2007; Kageyama
484 et al., 2013). One of these weaknesses is the underestimation of the spread of the African monsoon
485 towards North Africa. However, the increased discharge from the Nile river, induced by the enhanced
486 monsoon is well supported by data (Adamson et al., 1980; Revel et al., 2014; Williams, 2000).



487
 488
 489
 490
 491
 492

Figure 7: Temperature and precipitation deviations of EHOL from PICTRL in LMDZ-global, the AGCM for a) winter surface air temperatures at 2 m, b) summer surface air temperatures at 2 m, c) June to August precipitation, and d) July to September surface runoff (averaged over the entire simulation).

493 4.3 Mediterranean climate features with dynamical downscaling refinement

494 Figures 8, 9 and 10 show the results from the regional atmospheric model (LMDZ-regional), compared
 495 to those from LMDZ-global for PICTRL and EHOL over the Mediterranean region. In both the global
 496 and regional simulations, an increased seasonality is depicted, with warmer summer (+2 to +6 °C) and
 497 colder winter, especially over land (-3 to -1 °C, Figure 8). Downscaling with LMDZ-regional slightly
 498 reduces the amplitude of the summer warming and shows a more homogenous signal in winter over
 499 land. The general circulation of the surface wind in PICTRL is west to east (Figure 9b), in line with the
 500 dominant winter regime of westerlies in the region. This important feature is almost missed in the global
 501 model (Figure 9a) which reproduces a lower intensity than the regional model. The winter precipitation
 502 in EHOL, for ARCM (LMDZ-regional), increases over land in the Balkans and Italy and over the
 503 Adriatic, Ionian and Aegean Seas (Figure 10b). These changes are also present in the AGCM (LMDZ-

504 global) that, furthermore, shows an increase in Spain and Portugal (Figure 10a). It is in summer that the
505 two models show the largest differences. In ARCM (LMDZ-regional), the Mediterranean basin
506 experiences drier conditions, except in Italy and the North of the Balkans. Over the sea, precipitations
507 slightly increase in EHOL (Figure 10). However, the AGCM (LMDZ-global) shows drier conditions in
508 the northern two thirds of the Mediterranean domain, with more humid conditions in the southern third
509 (Figure 10c). Changes in precipitation lead to unavoidable modifications in the runoff and river
510 discharge into the Mediterranean Sea.

511

512 Although it is not straightforward to compare our “snapshot” simulations against environmental records
513 (often used to reconstruct a timeline), our results compare well with the available data for this area (see
514 supplementary online material, “Text S3: Comparison of model simulation outputs and reconstructed
515 data for the Mediterranean basin”). Numerous proxies provide information on lake levels, paleo fires,
516 pollen, isotopic signals recovered from speleothems which together describe the Mediterranean climate
517 in the past. All of these proxies need to be brought together to provide a clear impression of the
518 Mediterranean climate for this period (Magny et al., 2013; Peyron et al., 2011). Magny et al. (2007),
519 based on records from Lake Acessa (Italy), suggested that aridification took place around 9200–7700
520 cal BP. Zanchetta et al. (2007), based on data recovered from speleothems in Italy, conclude that the
521 Western Mediterranean basin experienced enhanced rainfall during the S1 (10000-7000 cal BP). Jalut
522 et al. (2009), using pollen data, suggest that the summers were short and dry and that there was abundant
523 rainfall in winter (autumn and spring as well) and remarked that these wetter conditions favoured broad-
524 leaf tree vegetation. Different proxies seem to provide contradictory information and therefore,
525 seasonality must be introduced to reconcile them. Peyron et al., (2011) mentioned wet winters and dry
526 summers during the ‘Holocene optimum’. Magny et al., (2013) support the hypothesis of seasonal
527 contrast based on the analysis of multi-proxies.

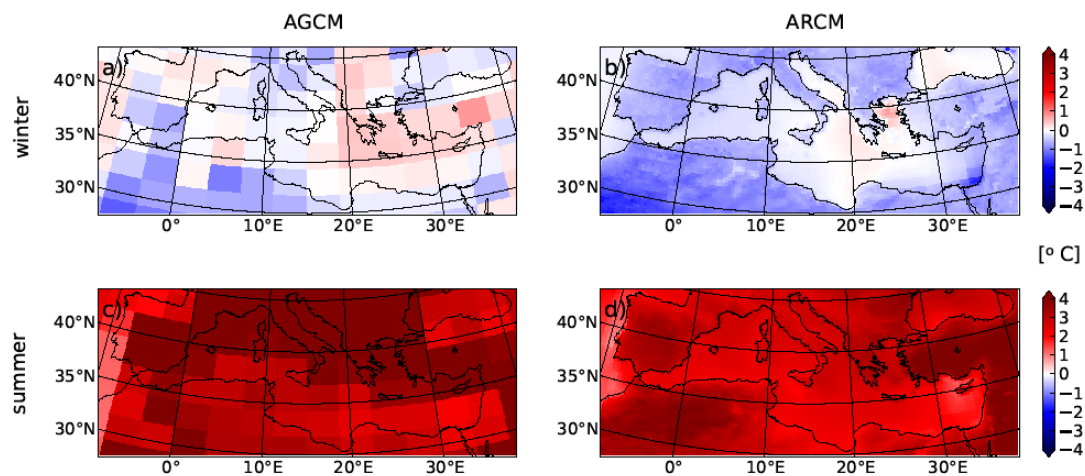
528

529 Our EHOL simulation successfully depicts this temperature contrast between winter and summer.
530 Precipitation is enhanced in winter. In summer, the Mediterranean region is globally drier, except over
531 Northern Italy and the northern Balkans. As explained above, there is no precipitation signal over
532 Northern Africa, although evidence of paleo-lakes has been found in Algeria (Callot and Fontugne,
533 1992; Petit-Maire et al., 1991), Tunisia (Fontes and Gasse, 1991) and Libya (Gaven et al., 1981; Lézine
534 and Casanova, 1991) during the Early Holocene indicating increased rainfall in this area. In the
535 supplementary material, a comparison between simulated continental precipitation outputs and pollen
536 reconstruction data is provided. This comparison shows that the winter precipitation anomalies are
537 consistent in both cases but that there is a distinct difference in summer values due to the more contrasted
538 summer in the EHOL simulation.

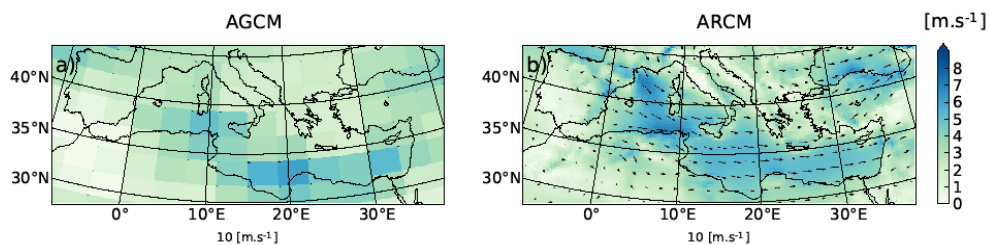
539

540

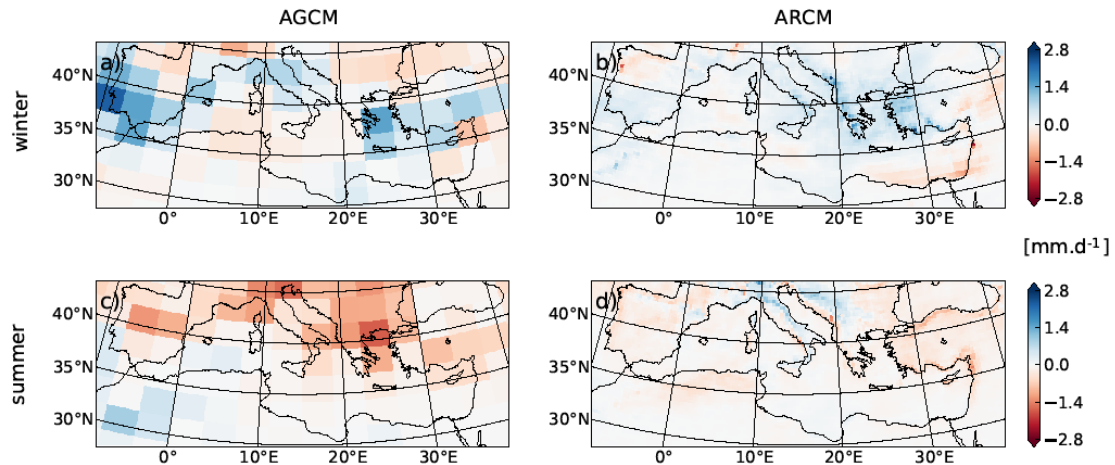
541
542



543
544 **Figure 8: Deviations (EHOL – PICTRL, averaged over the entire simulation) of surface air**
545 **temperature at 2 m for winter (upper panels) and summer (lower panels), respectively. AGCM**
546 **(LMDZ-global) is displayed on the left and ARCM (LMDZ-regional) on the right.**
547
548



549
550 **Figure 9: Winter wind-speed in PICTRL for a) the AGCM and b) the ARCM.**
551



552
 553 **Figure 10: Same as in Figure 8, but for precipitation rate (mm/day).**

554 **4.4 Hydrological changes**

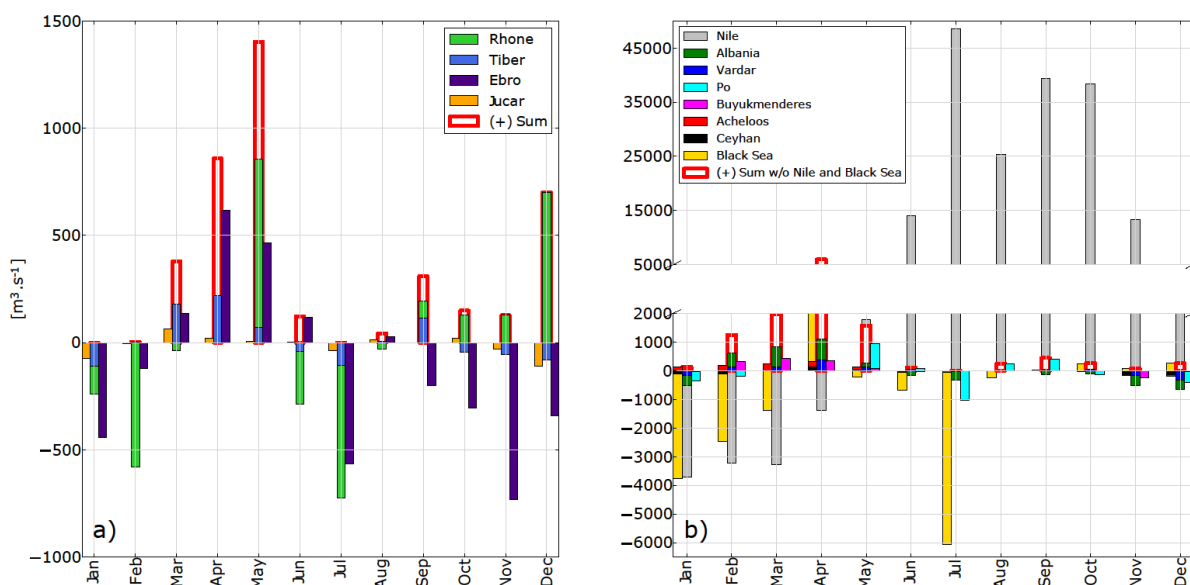
555
 556

557 Figure 11 shows anomalies (EHOL – PICTRL) of river freshwater supplies into the Mediterranean basin
 558 as simulated by the ARCM (LMDZ-regional). Bars are displayed for each calendar month to show the
 559 strong seasonal variation, and for the western and eastern basins separately. Due to their particular role
 560 and their specific treatment in our current modelling practice, the Nile and the Black Sea are also shown
 561 for the eastern basin, but not accounted in the sum. The North African rivers are not displayed since
 562 they don't show much changes for their catchment area. The Nile River shows important seasonal
 563 variation, with increase in summer and autumn and decrease in winter and spring. The Albanian rivers
 564 (Drini, Mat, Dures, Shkumbin and Vjosa) as well as the Vardar and the Buyukmenderes, produce
 565 positive anomalies in EHOL in winter, due to enhanced winter land precipitation in this simulation
 566 (Figure 10 b and d). The Black Sea net freshwater supply also changes in EHOL with important
 567 decreases in January, February, March and July, but increase in April. In EHOL, the supplementary
 568 winter freshwater input is less pronounced for the western basin than for the eastern basin (Figure 11b),
 569 but major rivers, such as Rhone and Ebro, do show a strong seasonal cycle. As a whole the western basin
 570 sees an increase of river discharges from March to June.

571 In terms of areal means for the entire Mediterranean draining basin, the different components of the
 572 freshwater budget are shown in Table 1 (bottom) for both PICTRL and EHOL, to be compared to the
 573 observation-based estimation OBS and the historical simulation HIST. From PICTRL to EHOL, the
 574 annual precipitation over the Mediterranean Sea itself does not change much, but the annual evaporation
 575 amount shows a slight increase (from 1031 to 1094 mm.year⁻¹). However, the most remarkable feature

576 is the increase of river discharges: 98 mm.year⁻¹ in PICTRL to 225 mm.year⁻¹ in EHOL. The total water
 577 deficit finally decreases from 378 to 305 mm.year⁻¹.

578
 579
 580
 581



582
 583 **Figure 11: Monthly anomalies (EHOL – PICTRL, with seasonal variation) of fresh water**
 584 **discharges ($\text{m}^3 \cdot \text{s}^{-1}$) for major rivers flowing into the western basin (left panel) and the eastern**
 585 **basin (right panel). The sum of all rivers for each basin is also plotted. The Nile and the Black Sea**
 586 **are also shown as rivers of the eastern basin, but not accounted into the basin-scale sum.**

587
 588

589 4.5 Changes in water properties of the Mediterranean Sea

590 At the end of our modelling chain, changes in the properties of the Mediterranean seawater produced by
 591 NEMOMED8 for PICTRL and EHOL are examined. It is important to mention at this stage, that for the
 592 correction of the river runoff the reference is the pre-industrial state, and not the historical simulation
 593 (as is the case for SST and SIC). Our aim was to keep river runoff anomalies free of anthropogenic
 594 influence. In addition, the fact that the “pre-industrial” Nile river runoff (in other words before
 595 damming) is well known influenced this choice. The procedure of river runoff correction is detailed in
 596 the supplementary material (Text S2: Bias correction). Figure 12 shows changes (EHOL minus
 597 PICTRL) for sea surface salinities, index of stratification and MLD for the last 30 years of simulation.
 598 The EHOL simulation reasonably reaches the steady state in terms of IS, ZOF and SSS, as shown in

599 Figures S6 to S8 of the supplementary material. The freshwater inputs from the Nile and the north-
600 eastern margin imply a lower salinity in the eastern basin. This decrease in salinity enhances
601 stratification throughout the Mediterranean Sea (with the exception of the Sicily Sea) and affects the
602 convection areas by decreasing the MLD, especially in the Gulf of Lions, in the Adriatic and Ionian Seas
603 and in the Aegean. Such a situation is expected and consistent with the basic climatology of MLD,
604 shown in Figure 5. This global stratification in EHOL is followed by a general reduction in the
605 thermohaline circulation compared to PICTRL (ZOF and MOF, Figure 13).

606

607 Numerous studies have documented the sapropel event S1 and the state of the Mediterranean Sea that
608 caused it. Emeis et al. (2000) mentioned a decreased SSS during this period in both the eastern and
609 western basins (as did Kallel et al., 1997 in the Tyrrhenian basin). In the subsection “*Sea Surface*
610 *Temperatures*” and “*Sea Surface Salinity*” of the section “Text S3” in the supplementary online material,
611 simulated SST and SSS to reconstructions are compared. Although simulated SST is in good agreement
612 with the reconstructed data, there is a gap between the simulated SSS and reconstructions. This
613 discrepancy is not surprising. Indeed, there are many explanations for the underestimation in our model
614 of the salinity. One of them is a common weakness in Early to Mid-Holocene simulations, namely, the
615 underestimation of the northward spread of the African monsoon and therefore, the underestimation of
616 the freshwater flow from North Africa. Adloff (2011), already pointed to a shortfall in freshwater input
617 to reconcile the simulated and observed SSS during the Early Holocene. Our oceanic simulation depicts
618 these behaviours well and is overall similar to previous modelling studies with lower resolution (Adloff
619 et al., 2011; Bosmans et al., 2015; Myers et al., 1998).

620

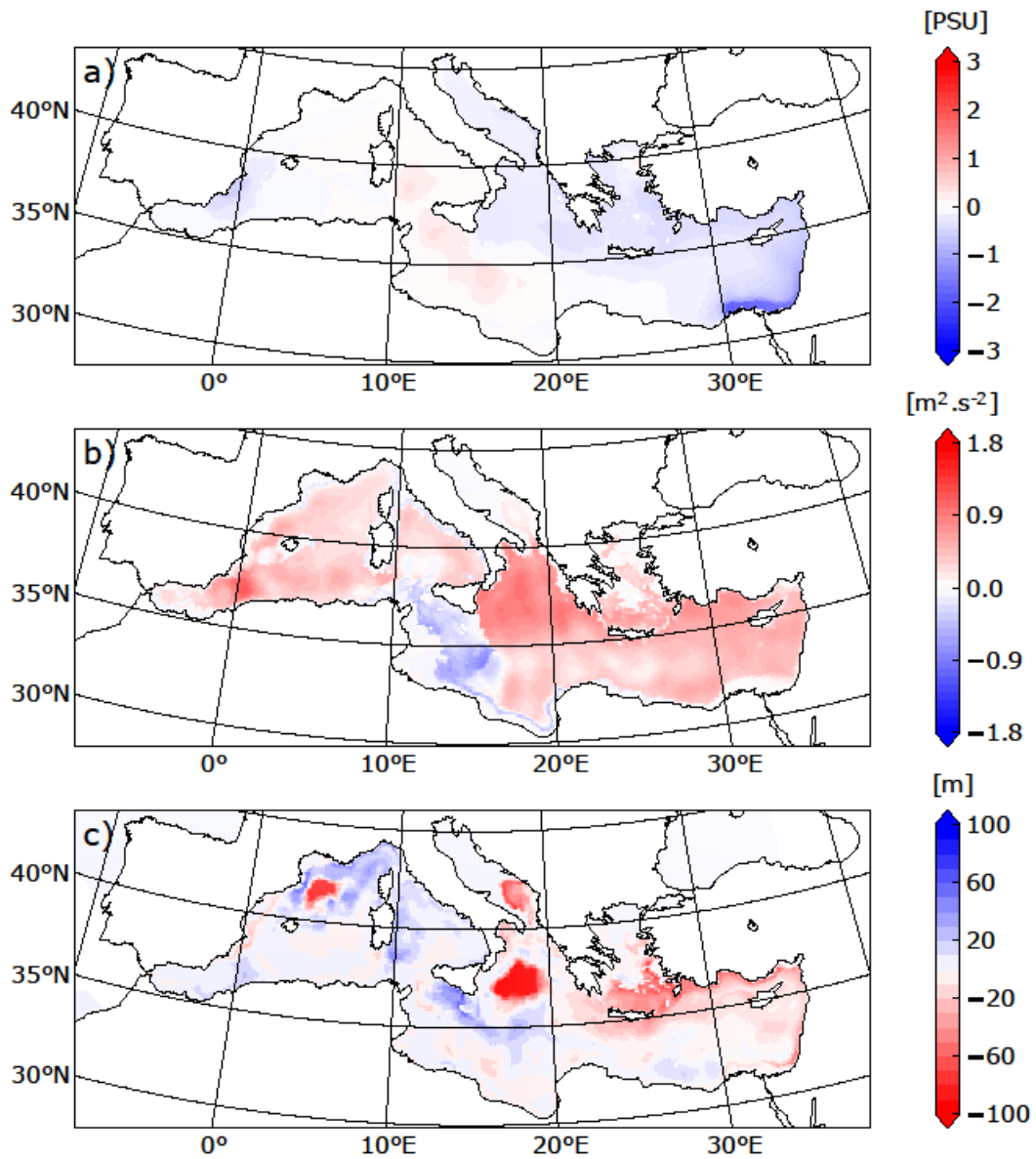
621 Two other issues need to be discussed for the Early Holocene. The first one is sea level, which was 20
622 metres lower than the present day (Peltier et al., 2015). For the sake of simplicity, this difference of sea
623 level is not taken into account in the EHOL simulation. The second issue is the timing of the
624 (re)connection between the Black Sea and the Aegean Sea. This topic is still being debated. Sperling et
625 al. (2003) suggested this reconnection occurred around 8.4 ka BP, while by the calculations of Soulet et
626 al. (2011) it happened around 9 ka BP. Other studies found that an overflow from the Black Sea likely
627 occurred before this reconnection due to Fennoscandian ice-sheet melting during the deglaciation
628 (Chepalyga, 2007; Major et al., 2002; Soulet et al., 2011). For the purposes of this work, the Bosphorus
629 is maintained open in EHOL simulation, with the water exchange set at its modern value.

630

631

632

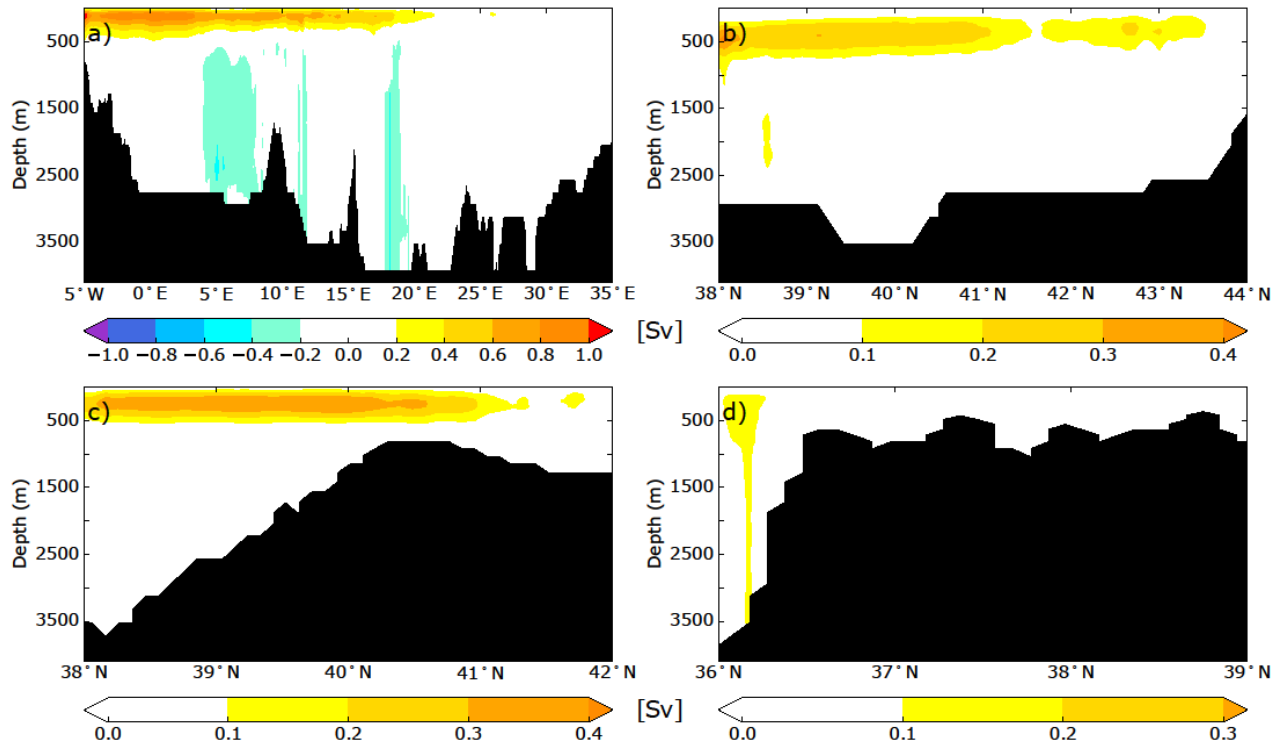
633



634

635 **Figure 12: Deviations between EHOL and PICTRL in a) sea surface salinity, b) index of**

636 **stratification, c) mixed-layer depth, averaged over the last 30 years of simulation**



637
 638 **Figure 13: ZOF (a) and MOF (b, Gulf of Lion, c, Adriatic/Ionian Sea, d, Aegean Sea) for EHOL**
 639 **experiment, averaged over the last 30 years of simulation. These overturning stream-functions**
 640 **were calculated in the same way as in Fig. 6, providing a strict comparison with the experiments**
 641 **HIST and PICTRL.**

642 5 Conclusion and perspectives for the modelling platform

643
 644 This study aimed to develop a modelling platform to simulate different climatic conditions of the
 645 Mediterranean basin. We developed a useful regional climate investigation platform with high spatial
 646 resolution over the Mediterranean region. This is particularly relevant for the study of impacts on the
 647 circulation of the Mediterranean Sea. The model chain has been evaluated for the historical period. We
 648 have presented Early Holocene simulations as an example of the potential of this platform to simulate
 649 past climate. For the Early Holocene, our model reproduced satisfactorily the global and regional climate
 650 features, compared to the observed data. Our platform allowed, for the first time, the generation of a
 651 high-resolution freshwater budget for this period, with a particular focus on continental precipitation, a
 652 key factor for the Mediterranean Sea in the assessment of its impact on circulation during the onset of
 653 the sapropel event, S1. An important limitation of our sequential approach is the fact that it does not
 654 take account of feedback of ocean changes on atmospheric circulation. However, this architecture allows
 655 eventual bias correction, conducted at different levels of the platform if needed. One way to overcome

656 this problem of interactive ocean would be to consider an “asynchronous mode”, namely, to take account
657 of feedback from the ocean component to the atmosphere at a yearly or decadal frequency.

658

659

660 The modelling sequence, moving from global simulation at low resolution to high-resolution regional
661 ocean modelling, avoids the problem of boundary conditions, and provides a fully consistent platform
662 that may be used for many paleoclimate studies. We focused here on the Early Holocene period but this
663 architecture could be used to study other periods investigated in MIPs, such as the Last Glacial
664 Maximum or the deposition of older sapropels, from the Pliocene to the Quaternary, as long as the
665 tectonics remain mainly unchanged (PMIP, PlioMIP).

666

667

668 **Code and data availability.** The current version of LMDZ and NEMO are available from the project
669 website: https://forge.ipsl.jussieu.fr/igcmg_doc/wiki/DocImodelBlmdz and
670 <http://forge.ipsl.jussieu.fr/nemo/wiki/Users> under the terms of the CeCill license for LMDZ and
671 NEMO both. The exact version of the model used to produce the results used in this paper is archived
672 on Zenodo (Vadsaria et al., 2019), as are input data and scripts to run the model and produce the plots
673 for all the simulations presented in this paper.

674

675 **Author’s contribution.** This study was co-designed and approved by all co-authors. The simulation
676 protocol was constructed by TV and LL from a modelling architecture provided by LL. TV conducted
677 the numerical simulations and drafted the first version of the manuscript. All co-authors are largely
678 involved in the writing and revision of the manuscript.

679

680 **Acknowledgments.** We thank Mary Minnock for her professional English revision. This work was
681 supported by the French National program LEFE “HoMoSapiENS”. This work was granted access to
682 the HPC resources of TGCC under the allocation 2017-A0010102212, 2018-A0030102212 and 2018-
683 A004-01-00239 made by GENCI.

684

685

686 **References**

687

688 Adamson, D. A., Gasse, F., Street, F. A. and Williams, M. A. J.: Late Quaternary history of the Nile,
689 Nature, 288(5786), 50–55, doi:10.1038/288050a0, 1980.

690

691 Adler, R., Sapiano, M., Huffman, G., Wang, J.-J., Gu, G., Bolvin, D., Chiu, L., Schneider, U., Becker,
692 A., Nelkin, E., Xie, P., Ferraro, R. and Shin, D.-B.: The Global Precipitation Climatology Project
693 (GPCP) Monthly Analysis (New Version 2.3) and a Review of 2017 Global Precipitation, Atmosphere
694 (Basel)., 9(4), 138, doi:10.3390/atmos9040138, 2018.

695

696 Adloff, F., Mikolajewicz, U., Kučera, M., Grimm, R., Maier-Reimer, E., Schmiedl, G. and Emeis, K.-
697 C.: Upper ocean climate of the Eastern Mediterranean Sea during the Holocene Insolation Maximum –
698 a model study" published in *Clim. Past*, 7, 1103–1122, 2011, *Clim. Past*, 7(4), 1149–1168,
699 doi:10.5194/cp-7-1149-2011, 2011.

700

701 Adloff, F., Somot, S., Sevault, F., Jordà, G., Aznar, R., Déqué, M., Herrmann, M., Marcos, M., Dubois,
702 C., Padorno, E., Alvarez-Fanjul, E. and Gomis, D.: Mediterranean Sea response to climate change in an
703 ensemble of twenty first century scenarios, *Clim. Dyn.*, 45(9–10), 2775–2802, doi:10.1007/s00382-015-
704 2507-3, 2015.

705

706 Artale, V.: Role of surface fluxes in ocean general circulation models using satellite sea surface
707 temperature: Validation of and sensitivity to the forcing frequency of the Mediterranean thermohaline
708 circulation, *J. Geophys. Res.*, 107(C8), 3120, doi:10.1029/2000JC000452, 2002.

709

710 Artale, V., Calmanti, S., Carillo, A., Dell’Aquila, A., Herrmann, M., Pisacane, G., Ruti, P. M., Sannino,
711 G., Struglia, M. V., Giorgi, F., Bi, X., Pal, J. S. and Rauscher, S.: An atmosphere–ocean regional climate
712 model for the Mediterranean area: assessment of a present climate simulation, *Clim. Dyn.*, 35(5), 721–
713 740, doi:10.1007/s00382-009-0691-8, 2010.

714

715 [Barnier, B., Siefridt, L. and Marchesiello, P.: Thermal forcing for a global ocean circulation model using](#)
716 [a three-year climatology of ECMWF analyses, *J. Mar. Syst.*, 6\(4\), 363–380, doi:10.1016/0924-](#)
717 [7963\(94\)00034-9, 1995.](#)

718

719 Béranger, K., Drillet, Y., Houssais, M.-N., Testor, P., Bourdallé-Badie, R., Alammoud, B., Bozec, A.,
720 Mortier, L., Bouruet-Aubertot, P. and Crépon, M.: Impact of the spatial distribution of the atmospheric
721 forcing on water mass formation in the Mediterranean Sea, *J. Geophys. Res.*, 115(C12), C12041,
722 doi:10.1029/2009JC005648, 2010.

723

724 Beuvier, J., Sevault, F., Herrmann, M., Kontoyiannis, H., Ludwig, W., Rixen, M., Stanev, E., Béranger,
725 K. and Somot, S.: Modeling the Mediterranean Sea interannual variability during 1961–2000: Focus on
726 the Eastern Mediterranean Transient, *J. Geophys. Res.*, 115(C8), C08017, doi:10.1029/2009JC005950,
727 2010.

728

729 Bosmans, J. H. C., Drijfhout, S. S., Tuenter, E., Lourens, L. J., Hilgen, F. J. and Weber, S. L.: Monsoonal
730 response to mid-holocene orbital forcing in a high resolution GCM, *Clim. Past*, 8(2), 723–740,
731 doi:10.5194/cp-8-723-2012, 2012.

732

733 Bosmans, J. H. C., Drijfhout, S. S., Tuenter, E., Hilgen, F. J., Lourens, L. J. and Rohling, E. J.: Precession
734 and obliquity forcing of the freshwater budget over the Mediterranean, *Quat. Sci. Rev.*, 123, 16–30,
735 doi:10.1016/j.quascirev.2015.06.008, 2015.

736

737 Braconnot, P., Otto-Bliesner, B., Harrison, S., Joussaume, S., Peterchmitt, J., Abe-Ouchi, A., Crucifix,
738 M., Driesschaert, E., Fichefet, T., Hewitt, C. D., Kageyama, M., Kitoh, A., Lâiné, A., Loutre, M., Marti,
739 O., Merkel, U., Ramstein, G., Valdes, P., Weber, S. L., Yu, Y. and Zhao, Y.: Results of PMIP2 coupled
740 simulations of the Mid-Holocene and Last Glacial Maximum – Part 1: experiments and
741 large-scale features, *Clim. Past*, 3(2), 261–277, doi:10.5194/cp-3-261-2007, 2007.

742

743 Callot, Y. and Fontugne, M.: Les étagements de nappes dans les paléolacs holocènes du nord-est du
744 Grand Erg Occidental (Algérie)., 1992.

745

746 Chen, J., Brissette, F. P. and Leconte, R.: Uncertainty of downscaling method in quantifying the impact
747 of climate change on hydrology, *J. Hydrol.*, 401(3–4), 190–202, doi:10.1016/j.jhydrol.2011.02.020,
748 2011.

749

750 Chepalyga, A. L.: The late glacial great flood in the Ponto-Caspian basin, in *The Black Sea Flood*
751 *Question: Changes in Coastline, Climate, and Human Settlement*, pp. 119–148, Springer Netherlands.,
752 2007.

753

754 Dee, D. P., Uppala, S. M., Simmons, A. J., Berrisford, P., Poli, P., Kobayashi, S., Andrae, U.,
755 Balmaseda, M. A., Balsamo, G., Bauer, P., Bechtold, P., Beljaars, A. C. M., van de Berg, L., Bidlot, J.,
756 Bormann, N., Delsol, C., Dragani, R., Fuentes, M., Geer, A. J., Haimberger, L., Healy, S. B., Hersbach,
757 H., Hólm, E. V., Isaksen, L., Kållberg, P., Köhler, M., Matricardi, M., McNally, A. P., Monge-Sanz, B.
758 M., Morcrette, J.-J., Park, B.-K., Peubey, C., de Rosnay, P., Tavolato, C., Thépaut, J.-N. and Vitart, F.:
759 The ERA-Interim reanalysis: configuration and performance of the data assimilation system, *Q. J. R.*
760 *Meteorol. Soc.*, 137(656), 553–597, doi:10.1002/qj.828, 2011.

761

762 Dell’Aquila, A., Calmanti, S., Ruti, P., Struglia, M., Pisacane, G., Carillo, A. and Sannino, G.: Effects
763 of seasonal cycle fluctuations in an A1B scenario over the Euro-Mediterranean region, *Clim. Res.*, 52(1),
764 135–157, doi:10.3354/cr01037, 2012.

765

766 Drobinski, P., Anav, A., Lebeaupin Brossier, C., Samson, G., Stéfanon, M., Bastin, S., Baklouti, M.,
767 Béranger, K., Beuvier, J., Bourdallé-Badie, R., Coquart, L., D'Andrea, F., de Noblet-Ducoudré, N.,
768 Diaz, F., Dutay, J.-C., Ethe, C., Foujols, M.-A., Khvorostyanov, D., Madec, G., Mancip, M., Masson,
769 S., Menut, L., Palmieri, J., Polcher, J., Turquety, S., Valcke, S. and Viovy, N.: Model of the Regional
770 Coupled Earth system (MORCE): Application to process and climate studies in vulnerable regions,
771 *Environ. Model. Softw.*, 35, 1–18, doi:10.1016/j.envsoft.2012.01.017, 2012.

772

773 Dufresne, J.-L., Foujols, M.-A., Denvil, S., Caubel, A., Marti, O., Aumont, O., Balkanski, Y., Bekki, S.,
774 Bellenger, H., Benschila, R., Bony, S., Bopp, L., Braconnot, P., Brockmann, P., Cadule, P., Cheruy, F.,
775 Codron, F., Cozic, A., Cugnet, D., de Noblet, N., Duvel, J.-P., Ethé, C., Fairhead, L., Fichefet, T.,
776 Flavoni, S., Friedlingstein, P., Grandpeix, J.-Y., Guez, L., Guilyardi, E., Hauglustaine, D., Hourdin, F.,
777 Idelkadi, A., Ghattas, J., Joussaume, S., Kageyama, M., Krinner, G., Labetoulle, S., Lahellec, A.,
778 Lefebvre, M.-P., Lefevre, F., Levy, C., Li, Z. X., Lloyd, J., Lott, F., Madec, G., Mancip, M., Marchand,
779 M., Masson, S., Meurdesoif, Y., Mignot, J., Musat, I., Parouty, S., Polcher, J., Rio, C., Schulz, M.,
780 Swingedouw, D., Szopa, S., Talandier, C., Terray, P., Viovy, N. and Vuichard, N.: Climate change
781 projections using the IPSL-CM5 Earth System Model: from CMIP3 to CMIP5, *Clim. Dyn.*, 40(9–10),
782 2123–2165, doi:10.1007/s00382-012-1636-1, 2013.

783

784 Emeis, K.-C., Struck, U., Schulz, H.-M., Rosenberg, R., Bernasconi, S., Erlenkeuser, H., Sakamoto, T.
785 and Martinez-Ruiz, F.: Temperature and salinity variations of Mediterranean Sea surface waters over
786 the last 16,000 years from records of planktonic stable oxygen isotopes and alkenone unsaturation ratios,
787 *Palaeogeogr. Palaeoclimatol. Palaeoecol.*, 158(3–4), 259–280, doi:10.1016/S0031-0182(00)00053-5,
788 2000.

789

790 Fontes, J. C. and Gasse, F.: PALHYDAF (Palaeohydrology in Africa) program: objectives, methods,
791 major results, *Palaeogeogr. Palaeoclimatol. Palaeoecol.*, 84(1–4), 191–215, doi:10.1016/0031-
792 0182(91)90044-R, 1991.

793

794 Gaven, C., Hillaire-Marcel, C. and Petit-Maire, N.: A Pleistocene lacustrine episode in southeastern
795 Libya, *Nature*, 290(5802), 131–133, doi:10.1038/290131a0, 1981.

796

797 Giorgi, F.: Climate change hot-spots, *Geophys. Res. Lett.*, 33(8), L08707, doi:10.1029/2006GL025734,
798 2006.

799

800 Goubanova, K. and Li, L.: Extremes in temperature and precipitation around the Mediterranean basin
801 in an ensemble of future climate scenario simulations, *Glob. Planet. Change*, 57(1–2), 27–42,

802 doi:10.1016/j.gloplacha.2006.11.012, 2007.
803

804 Harrison, S. P., Bartlein, P. J., Brewer, S., Prentice, I. C., Boyd, M., Hessler, I., Holmgren, K., Izumi,
805 K. and Willis, K.: Climate model benchmarking with glacial and mid-Holocene climates, *Clim. Dyn.*,
806 43(3–4), 671–688, doi:10.1007/s00382-013-1922-6, 2014.
807

808 Hernández-Díaz, L., Laprise, R., Nikiéma, O. and Winger, K.: 3-Step dynamical downscaling with
809 empirical correction of sea-surface conditions: application to a CORDEX Africa simulation, *Clim. Dyn.*,
810 48(7–8), 2215–2233, doi:10.1007/s00382-016-3201-9, 2017.
811

812 Herrmann, M., Sevault, F., Beuvier, J. and Somot, S.: What induced the exceptional 2005 convection
813 event in the northwestern Mediterranean basin? Answers from a modeling study, *J. Geophys. Res.*,
814 115(C12), C12051, doi:10.1029/2010JC006162, 2010.
815

816 Houpert, L., Testor, P., Durrieu de Madron, X., Somot, S., D’Ortenzio, F., Estournel, C. and Lavigne,
817 H.: Seasonal cycle of the mixed layer, the seasonal thermocline and the upper-ocean heat storage rate in
818 the Mediterranean Sea derived from observations, *Prog. Oceanogr.*, 132, 333–352,
819 doi:10.1016/j.pocean.2014.11.004, 2015.
820

821 Hourdin, F., Musat, I., Bony, S., Braconnot, P., Codron, F., Dufresne, J.-L., Fairhead, L., Filiberti, M.-
822 A., Friedlingstein, P., Grandpeix, J.-Y., Krinner, G., LeVan, P., Li, Z.-X. and Lott, F.: The LMDZ4
823 general circulation model: climate performance and sensitivity to parametrized physics with emphasis
824 on tropical convection, *Clim. Dyn.*, 27(7–8), 787–813, doi:10.1007/s00382-006-0158-0, 2006.
825

826 Jalut, G., Dedoubat, J. J., Fontugne, M. and Otto, T.: Holocene circum-Mediterranean vegetation
827 changes: Climate forcing and human impact, *Quat. Int.*, 200(1–2), 4–18,
828 doi:10.1016/j.quaint.2008.03.012, 2009.
829

830 Jost, A., Lunt, D., Kageyama, M., Abe-Ouchi, A., Peyron, O., Valdes, P. J. and Ramstein, G.: High-
831 resolution simulations of the last glacial maximum climate over Europe: a solution to discrepancies with
832 continental palaeoclimatic reconstructions?, *Clim. Dyn.*, 24(6), 577–590, doi:10.1007/s00382-005-
833 0009-4, 2005.
834

835 Kageyama, M., Braconnot, P., Bopp, L., Caubel, A., Foujols, M.-A., Guilyardi, E., Khodri, M., Lloyd,
836 J., Lombard, F., Mariotti, V., Marti, O., Roy, T. and Woillez, M.-N.: Mid-Holocene and Last Glacial
837 Maximum climate simulations with the IPSL model—part I: comparing IPSL_CM5A to IPSL_CM4,
838 *Clim. Dyn.*, 40(9–10), 2447–2468, doi:10.1007/s00382-012-1488-8, 2013.

839
840
841
842
843
844
845
846
847
848
849
850
851
852
853
854
855
856
857
858
859
860
861
862
863
864
865
866
867
868
869
870
871
872
873
874
875

Kallel, N., Paterne, M., Labeyrie, L., Duplessy, J.-C. and Arnold, M.: Temperature and salinity records of the Tyrrhenian Sea during the last 18,000 years, *Palaeogeogr. Palaeoclimatol. Palaeoecol.*, 135(1–4), 97–108, doi:10.1016/S0031-0182(97)00021-7, 1997.

Kourafalou, V. H. and Barbopoulos, K.: High resolution simulations on the North Aegean Sea seasonal circulation, *Ann. Geophys.*, 21(1), 251–265, doi:10.5194/angeo-21-251-2003, 2003.

Krinner, G., Viovy, N., de Noblet-Ducoudré, N., Ogée, J., Polcher, J., Friedlingstein, P., Ciais, P., Sitch, S. and Prentice, I. C.: A dynamic global vegetation model for studies of the coupled atmosphere-biosphere system, *Global Biogeochem. Cycles*, 19(1), 1–33, doi:10.1029/2003GB002199, 2005.

Krinner, G., Llargeron, C., Ménégoz, M., Agosta, C. and Brutel-Vuilmet, C.: Oceanic Forcing of Antarctic Climate Change: A Study Using a Stretched-Grid Atmospheric General Circulation Model, *J. Clim.*, 27(15), 5786–5800, doi:10.1175/JCLI-D-13-00367.1, 2014.

Krinner, G., Beaumet, J., Favier, V., Déqué, M. and Brutel-Vuilmet, C.: Empirical Run-Time Bias Correction for Antarctic Regional Climate Projections With a Stretched-Grid AGCM, *J. Adv. Model. Earth Syst.*, 11(1), 64–82, doi:10.1029/2018MS001438, 2019.

Lacombe, H. and Tchernia, P.: Caractères hydrologiques et circulation des eaux en Méditerranée., in *The Mediterranean Sea: A natural sedimentation laboratory*, edited by D. . Stanley, pp. 25–36, Dowden, Hutchinson & Ross, Stroudsburg., 1972.

De Lange, G. J., Thomson, J., Reitz, A., Slomp, C. P., Speranza Principato, M., Erba, E. and Corselli, C.: Synchronous basin-wide formation and redox-controlled preservation of a Mediterranean sapropel, *Nat. Geosci.*, 1(9), 606–610, doi:10.1038/ngeo283, 2008.

Lebeaupin Brossier, C., Béranger, K., Deltel, C. and Drobinski, P.: The Mediterranean response to different space–time resolution atmospheric forcings using perpetual mode sensitivity simulations, *Ocean Model.*, 36(1–2), 1–25, doi:10.1016/j.ocemod.2010.10.008, 2011.

Lézine, A.-M. and Casanova, J.: Correlated oceanic and continental records demonstrate past climate and hydrology of North Africa (0-140 ka), *Geology*, 19(4), 307–310, doi:10.1130/0091-7613(1991)019<0307:COACRD>2.3.CO;2, 1991.

Li, L., Bozec, A., Somot, S., Bouruet-Aubertot, P. and Crepon, M.: Regional atmospheric, marine

876 processes and climate modelling, in *Mediterranean climate variability and predictability*, edited by P.
877 Lionello, P. Malanotte-Rizzoli, and R. Boscolo, Elsevier., 2006.
878

879 Li, L., Casado, A., Congedi, L., Dell’Aquila, A., Dubois, C., Elizalde, A., L’Hévéder, B., Lionello, P.,
880 Sevault, F., Somot, S., Ruti, P. and Zampieri, M.: Modeling of the mediterranean climate system, in *The*
881 *Climate of the Mediterranean Region*, pp. 419–448, Elsevier Inc., 2012.
882

883 Li, Z.-X.: Ensemble Atmospheric GCM Simulation of Climate Interannual Variability from 1979 to
884 1994, *J. Clim.*, 12(4), 986–1001, doi:10.1175/1520-0442(1999)012<0986:EAGSOC>2.0.CO;2, 1999.

885 Locarnini, R. A., Mishonov, A. V., Antonov, J. I., Boyer, T. P., Garcia, H. E., Baranova, O. K., Zweng,
886 M. M., Paver, C. R., Reagan, J. R., Johnson, D. R., Hamilton, M. and Seidov, D.: *World Ocean Atlas*
887 2013. Vol. 1: Temperature., S. Levitus, Ed.; A. Mishonov, Tech. Ed.; NOAA Atlas NESDIS,
888 73(September), 40, doi:10.1182/blood-2011-06-357442, 2013.
889

890 Ludwig, P., Shao, Y., Kehl, M. and Weniger, G.-C.: The Last Glacial Maximum and Heinrich event I
891 on the Iberian Peninsula: A regional climate modelling study for understanding human settlement
892 patterns, *Glob. Planet. Change*, 170, 34–47, doi:10.1016/j.gloplacha.2018.08.006, 2018.
893

894 Ludwig, W., Dumont, E., Meybeck, M. and Heussner, S.: River discharges of water and nutrients to the
895 Mediterranean and Black Sea: Major drivers for ecosystem changes during past and future decades?,
896 *Prog. Oceanogr.*, 80(3–4), 199–217, doi:10.1016/j.pocean.2009.02.001, 2009.
897

898 Macias, D. M., Garcia-Goriz, E. and Stips, A.: Productivity changes in the Mediterranean Sea for the
899 twenty-first century in response to changes in the regional atmospheric forcing, *Front. Mar. Sci.*, 2,
900 doi:10.3389/fmars.2015.00079, 2015.
901

902 Madec, G.: *NEMO ocean engine-version 3.0-Laboratoire d’Océanographie et du Climat:*
903 *Expérimentation et Approches Numériques*, 2008.
904

905 Magny, M., de Beaulieu, J.-L., Drescher-Schneider, R., Vannière, B., Walter-Simonnet, A.-V., Miras,
906 Y., Millet, L., Bossuet, G., Peyron, O., Brugiapaglia, E. and Leroux, A.: Holocene climate changes in
907 the central Mediterranean as recorded by lake-level fluctuations at Lake Accessa (Tuscany, Italy), *Quat.*
908 *Sci. Rev.*, 26(13–14), 1736–1758, doi:10.1016/j.quascirev.2007.04.014, 2007.
909

910 Magny, M., Combourieu-Nebout, N., de Beaulieu, J. L., Bout-Roumazeilles, V., Colombaroli, D.,
911 Desprat, S., Francke, A., Joannin, S., Ortu, E., Peyron, O., Revel, M., Sadori, L., Siani, G., Sicre, M. A.,
912 Samartin, S., Simonneau, A., Tinner, W., Vannière, B., Wagner, B., Zanchetta, G., Anselmetti, F.,

913 Brugiapaglia, E., Chapron, E., Debret, M., Desmet, M., Didier, J., Essallami, L., Galop, D., Gilli, A.,
914 Haas, J. N., Kallel, N., Millet, L., Stock, A., Turon, J. L. and Wirth, S.: North&ndash;south
915 palaeohydrological contrasts in the central Mediterranean during the Holocene: tentative synthesis and
916 working hypotheses, *Clim. Past*, 9(5), 2043–2071, doi:10.5194/cp-9-2043-2013, 2013.

917

918 Major, C., Ryan, W., Lericolais, G. and Hajdas, I.: Constraints on Black Sea outflow to the Sea of
919 Marmara during the last glacial–interglacial transition, *Mar. Geol.*, 190(1–2), 19–34,
920 doi:10.1016/S0025-3227(02)00340-7, 2002.

921

922 Marzin, C. and Braconnot, P.: Variations of Indian and African monsoons induced by insolation changes
923 at 6 and 9.5 kyr BP, *Clim. Dyn.*, 33(2–3), 215–231, doi:10.1007/s00382-009-0538-3, 2009.

924 Mikolajewicz, U.: Modeling Mediterranean Ocean climate of the Last Glacial Maximum, *Clim. Past*,
925 7(1), 161–180, doi:10.5194/cp-7-161-2011, 2011.

926

927 Millot, C. and Taupier-Letage, I.: Circulation in the Mediterranean Sea, pp. 29–66., 2005.

928 Myers, P. G., Haines, K. and Rohling, E. J.: Modeling the paleocirculation of the Mediterranean: The
929 Last Glacial Maximum and the Holocene with emphasis on the formation of sapropel S 1,
930 *Paleoceanography*, 13(6), 586–606, doi:10.1029/98PA02736, 1998.

931

932 Peltier, W. R., Argus, D. F. and Drummond, R.: Space geodesy constrains ice age terminal deglaciation:
933 The global ICE-6G_C (VM5a) model, *J. Geophys. Res. Solid Earth*, 120(1), 450–487,
934 doi:10.1002/2014JB011176, 2015.

935

936 Petit-Maire, N., Fontugne, M. and Rouland, C.: Atmospheric methane ratio and environmental change
937 in the Sahara an Sahel during the last 130 kyrs, *Palaeogeogr. Palaeoclimatol. Palaeoecol.*, 86(1–2), 197–
938 206, doi:10.1016/0031-0182(91)90009-G, 1991.

939

940 Peyron, O., Goring, S., Dormoy, I., Kotthoff, U., Pross, J., de Beaulieu, J.-L., Drescher-Schneider, R.,
941 Vanni re, B. and Magny, M.: Holocene seasonality changes in the central Mediterranean region
942 reconstructed from the pollen sequences of Lake Accesa (Italy) and Tenaghi Philippon (Greece), *The*
943 *Holocene*, 21(1), 131–146, doi:10.1177/0959683610384162, 2011.

944

945 Pinardi, N., Cessi, P., Borile, F. and Wolfe, C. L. P.: The Mediterranean sea overturning circulation, *J.*
946 *Phys. Oceanogr.*, 49(7), 1699–1721, doi:10.1175/JPO-D-18-0254.1, 2019.

947

948 Ramstein, G., Kageyama, M., Guiot, J., Wu, H., H ely, C., Krinner, G. and Brewer, S.: How cold was
949 Europe at the Last Glacial Maximum? A synthesis of the progress achieved since the first PMIP model-

950 data comparison, *Clim. Past*, 3(2), 331–339, doi:10.5194/cp-3-331-2007, 2007.

951

952 Revel, M., Colin, C., Bernasconi, S., Combourieu-Nebout, N., Ducassou, E., Grousset, F. E., Rolland,
953 Y., Migeon, S., Bosch, D., Brunet, P., Zhao, Y. and Mascle, J.: 21,000 Years of Ethiopian African
954 monsoon variability recorded in sediments of the western Nile deep-sea fan, *Reg. Environ. Chang.*,
955 14(5), 1685–1696, doi:10.1007/s10113-014-0588-x, 2014.

956

957 Rossignol-Strick, M., Nesteroff, W., Olive, P. and Vergnaud-Grazzini, C.: After the deluge:
958 Mediterranean stagnation and sapropel formation, *Nature*, 295(5845), 105–110, doi:10.1038/295105a0,
959 1982.

960

961 Sanchez-Gomez, E., Somot, S., Josey, S. A., Dubois, C., Elguindi, N. and Déqué, M.: Evaluation of
962 Mediterranean Sea water and heat budgets simulated by an ensemble of high resolution regional climate
963 models, *Clim. Dyn.*, 37(9–10), 2067–2086, doi:10.1007/s00382-011-1012-6, 2011.

964

965 Sevault, F., Somot, S., Alias, A., Dubois, C., Lebeaupin-Brossier, C., Nabat, P., Adloff, F., Déqué, M.
966 and Decharme, B.: A fully coupled Mediterranean regional climate system model: design and evaluation
967 of the ocean component for the 1980–2012 period, *Tellus A Dyn. Meteorol. Oceanogr.*, 66(1), 23967,
968 doi:10.3402/tellusa.v66.23967, 2014.

969

970 Somot, S., Sevault, F. and Déqué, M.: Transient climate change scenario simulation of the
971 Mediterranean Sea for the twenty-first century using a high-resolution ocean circulation model, *Clim.*
972 *Dyn.*, 27(7–8), 851–879, doi:10.1007/s00382-006-0167-z, 2006.

973

974 Somot, S., Sevault, F., Déqué, M. and Crépon, M.: 21st century climate change scenario for the
975 Mediterranean using a coupled atmosphere–ocean regional climate model, *Glob. Planet. Change*, 63(2–
976 3), 112–126, doi:10.1016/j.gloplacha.2007.10.003, 2008.

977

978 Soulet, G., Ménot, G., Garreta, V., Rostek, F., Zaragosi, S., Lericolais, G. and Bard, E.: Black Sea
979 “Lake” reservoir age evolution since the Last Glacial — Hydrologic and climatic implications, *Earth*
980 *Planet. Sci. Lett.*, 308(1–2), 245–258, doi:10.1016/j.epsl.2011.06.002, 2011.

981

982 Sperling, M., Schmiedl, G., Hemleben, C., Emeis, K. ., Erlenkeuser, H. and Grootes, P. .: Black Sea
983 impact on the formation of eastern Mediterranean sapropel S1? Evidence from the Marmara Sea,
984 *Palaeogeogr. Palaeoclimatol. Palaeoecol.*, 190, 9–21, doi:10.1016/S0031-0182(02)00596-5, 2003.

985

986 Stanev, E. V., Le Traon, P.-Y. and Peneva, E. L.: Sea level variations and their dependency on

987 meteorological and hydrological forcing: Analysis of altimeter and surface data for the Black Sea, J.
988 Geophys. Res. Ocean., 105(C7), 17203–17216, doi:10.1029/1999JC900318, 2000.
989

990 Stickler, A., Brönnimann, S., Valente, M. A., Bethke, J., Sterin, A., Jourdain, S., Roucaute, E., Vasquez,
991 M. V., Reyes, D. A., Allan, R. and Dee, D.: ERA-CLIM: Historical Surface and Upper-Air Data for
992 Future Reanalyses, Bull. Am. Meteorol. Soc., 95(9), 1419–1430, doi:10.1175/BAMS-D-13-00147.1,
993 2014.
994

995 Swingedouw, D., Colin, C., Eynaud, F., Ayache, M. and Zaragosi, S.: Impact of freshwater release in
996 the Mediterranean Sea on the North Atlantic climate, Clim. Dyn., 53(7–8), 3893–3915,
997 doi:10.1007/s00382-019-04758-5, 2019.
998

999 Vadsaria, T., Li, L., Ramstein, G. and Dutay, J.-C.: Model and output for Vadsaria et al, “Development
1000 of a sequential tool LMDZ-NEMO-med-V1 for global to regional past climate simulation over the
1001 Mediterranean basin: an early Holocene case study”, GMD publication, ,
1002 doi:10.5281/ZENODO.3258410, 2019.
1003

1004 Vorosmarty, C. J., Feteke, B. M. and Tucker, B. A.: Global River Discharge, 1807-1991, V. 1.1
1005 (RivDIS), , doi:https://doi.org/10.3334/ORNLDAAC/199, 1998.
1006

1007 Williams, M.: Late Quaternary environments in the White Nile region, Sudan, Glob. Planet. Change,
1008 26(1–3), 305–316, doi:10.1016/S0921-8181(00)00047-3, 2000.
1009

1010 Zanchetta, G., Drysdale, R. N., Hellstrom, J. C., Fallick, A. E., Isola, I., Gagan, M. K. and Pareschi, M.
1011 T.: Enhanced rainfall in the Western Mediterranean during deposition of sapropel S1: stalagmite
1012 evidence from Corchia cave (Central Italy), Quat. Sci. Rev., 26(3–4), 279–286,
1013 doi:10.1016/j.quascirev.2006.12.003, 2007.
1014

1015 de Zolt, S., Lionello, P. and Malguzzi, P.: Implementation of an aorc in the mediterranean sea, 2003.
1016 Zweng, M. M., Reagan, J. R., Antonov, J. I., Mishonov, A. V., Boyer, T. P., Garcia, H. E., Baranova,
1017 O. K., Johnson, D. R., Seidov, D. and Bidlle, M. M.: World Ocean Atlas 2013, Volume 2: Salinity,
1018 NOAA Atlas NESDIS, 2(1), 39, doi:10.1182/blood-2011-06-357442, 2013.
1019